Journal of Medicinal Chemistry

Article

Mono-acidic inhibitors of the Kelch-like ECH-associated protein 1 : Nuclear factor erythroid 2–related factor 2 (KEAP1:NRF2) protein-protein interaction with high cell potency identified by Fragment-based Discovery

Thomas G. Davies, William E Wixted, Joseph E. Coyle, Charlotte Griffiths-Jones, Keisha Hearn, Rachel L. McMenamin, David Norton, Sharna J. Rich, Caroline Richardson, Gordon Saxty, Henriette Maria Gerarda Willems, Alison J.-A. Woolford, Joshua E. Cottom, Jen-Pyng Kou, John G. Yonchuk, Heidi G. Feldser, Yolanda Sanchez, Joseph P Foley, Brian J. Bolognese, Gregory A Logan, Patricia L. Podolin, Hongxing Yan, James F Callahan, Tom Daniel Heightman, and Jeffrey K Kerns

J. Med. Chem., **Just Accepted Manuscript** • DOI: 10.1021/acs.jmedchem.6b00228 • Publication Date (Web): 31 Mar 2016

Just Accepted

ACS Publications

Journal of Medicinal Chemistry is published by the American Chemical Society. 1155 Sixteenth Street N.W., Washington, DC 20036

Mono-acidic inhibitors of the Kelch-like ECH-associated protein 1 : Nuclear factor erythroid 2–related factor 2 (KEAP1:NRF2) protein-protein interaction with high cell potency identified by Fragment-based Discovery

Thomas G. Davies[1†], William E. Wixted[2†], Joseph E. Coyle[1], Charlotte Griffiths-Jones[1], Keisha Hearn[1], Rachel McMenamin[1], David Norton[1], Sharna J. Rich[1], Caroline Richardson[1], Gordon Saxty[1], Henriëtte M. G. Willems[1], Alison J.-A. Woolford[1], Joshua E. Cottom[3], Jen-Pyng Kou[2], John G. Yonchuk[2], Heidi G. Feldser[2], Yolanda Sanchez[2], Joseph P. Foley[2], Brian J. Bolognese[2], Gregory Logan[2], Patricia L. Podolin[2], Hongxing Yan[2], James F. Callahan[2], Tom D. Heightman[1]*, Jeffrey K. Kerns[2]*

[1]Astex Pharmaceuticals, 436 Cambridge Science Park, Cambridge, CB4 0QA, UK

[2]GlaxoSmithKline Pharmaceuticals, 709 Swedeland Road, King of Prussia, PA 19406, USA

[3]GlaxoSmithKline Pharmaceuticals, 1250 South Collegeville Road, Collegeville, PA 19426, USA

* Corresponding authors

† Co-first authors

ABSTRACT

KEAP1 is the key regulator of the NRF2-mediated cytoprotective response, and increasingly recognized as a target for diseases involving oxidative stress. Pharmacological intervention has focussed on molecules that decrease NRF2-ubiquitination through covalent modification of KEAP1 cysteine residues, but such electrophilic compounds lack selectivity and may be associated with off-target toxicity. We report here the first use of a fragment-based approach to directly target the KEAP1 Kelch–NRF2 interaction. X-ray crystallographic screening identified three distinct "hot-spots" for fragment binding within the NRF2 binding pocket of KEAP1, allowing progression of a weak fragment hit to molecules with nanomolar affinity for KEAP1 whilst maintaining drug-like properties. This work resulted in a promising lead compound which exhibits tight and selective binding to KEAP1, and activates the NRF2 antioxidant response in cellular and *in vivo* models, thereby providing a high quality chemical probe to explore the therapeutic potential of disrupting the KEAP1-NRF2 interaction.

INTRODUCTION

Living organisms are routinely exposed to reactive oxidants and electrophiles, both from internal metabolism and environmental toxins. Reactive oxygen and nitrogen species can elicit harmful oxidative stress, yet their controlled production is an essential component of cell signalling, necessitating a complex antioxidant regulatory network. The Nuclear factor erythroid 2–related factor 2 (NRF2) has emerged as a master regulator of cellular resistance to oxidants, mediating the up-regulation of multiple phase 2 and cytoprotective enzymes and proteins (e.g., NAD(P)H:quinone acceptor oxidoreductase 1 (NQO1) in response to electrophilic and oxidative assault.[1-3]

The protein Kelch-like ECH-associated protein 1 (KEAP1) plays a key role in the regulation of NRF2.[4] It consists of three domains: an N-terminal Broad-complex, Tramtrack and Bric-a-Brac (BTB) domain, serving as an adaptor for the E3 ubiquitin ligase Cul3/Rbx1; an Intervening Region (IVR) or BACK domain; and a C-terminal Kelch repeat domain, which is a protein-recognition module for NRF2 with a β-propeller fold (Figure 1a).[5-8] Under basal conditions, NRF2 is sequestered by the dimeric KEAP1/Cul3 complex, becoming ubiquitinated and degraded by the proteasome. An increase in levels of electrophilic species results in covalent modification of cysteine residues in the BTB and IVR domains, and leads to dissociation of Cul3 and other conformational changes.[2,4,9-12] This perturbs the ubiquitination of NRF2, allowing translocation to the nucleus where it activates antioxidant response elements (AREs) to increase expression of cytoprotective proteins.[13,14] Inadequate NRF2 signalling in the face of chronic oxidative stress has been proposed as a pathological mechanism in inflammatory diseases; up-

regulation of the pathway might be beneficial in a range of therapeutic areas including cardiovascular, neurodegeneration, and respiratory (e.g., chronic obstructive pulmonary disease) conditions.[15-19] Several electrophilic small molecules that covalently modify the KEAP1 cysteine residues responsible for sensing oxidative stress show clinical promise.[20] These include derivatives of the triterpenoid 2-cyano-3,12-dioxooleana-1,9-dien-28-oic-acid (CDDO),[21] the naturally occurring isothiocyanate sulforaphane,[22] and dimethyl fumarate which was recently approved by the FDA for the treatment of multiple sclerosis.[23]

The direct, non-covalent antagonism of the Kelch-NRF2 interaction (Figure 1b) may offer advantages including a larger therapeutic index. NRF2 binds two Kelch subunits in the KEAP1 dimer through high affinity ("ETGE") and low affinity ("DLG")[24-28] motifs which interact with a bowl-shaped pocket at the centre of the β-propeller fold; a cell-penetrant peptide containing the "ETGE" motif was recently reported to up-regulate protein levels associated with the anti-oxidant response.[29] A number of small molecules binding at the Kelch-NRF2 site have also been identified,[30-37] and although encouraging levels of affinity have been achieved[33] they show either weak activity in cells or are poorly drug-like. This is likely due to the presence of multiple arginine residues in the NRF2-binding site (Arg 380, Arg 415 and Arg 483), favouring the binding of poorly cell-permeable compounds containing multiple carboxylic acids that mimic the ETGE motif and its interactions with the Kelch domain (Figure 1c).

We report here the development of a small molecule inhibitor of the KEAP1 Kelch/NRF2 protein-protein interaction using a fragment-based drug discovery (FBDD) approach. The screen identified three distinct "hot-spots" for fragment binding within the NRF2 binding pocket of KEAP1, providing information on preferred interactions in these subsites which was used to progress a weak fragment hit (K_d >1 mM) to molecules with nanomolar affinity for KEAP1. The

lead compound KI-696 (compound **7**, Table 1) exhibits tight and selective binding to the Kelch domain, high potency in cell-based assays, and activation of the NRF2 pathway in animal models. It therefore provides a well validated *in vivo* active chemical probe with which to explore the therapeutic potential of disrupting the Kelch/NRF2 interface.

RESULTS

Identification of a potent and selective inhibitor of the KEAP1 Kelch/NRF2 interaction

It is well known that identifying protein-protein interaction inhibitors with favourable drug-like properties is challenging, and fragment-based approaches are increasingly recognised as a means of generating potent and selective inhibitors with good ligand efficiency.[38,39]

To enable X-ray crystallography as a primary screen, we used a mouse KEAP1 Kelch crystal system which possesses an NRF2 binding site unoccluded by crystal contacts, and suitable for high-throughput soaking experiments. A crystallographic screen of approximately 330 fragments led to the observation of binding in three discrete hot-spots within the NRF2 site, as exemplified by compounds **1**, **2** and **3**, which form interactions in the vicinity of Arg 483, Tyr 525 and Ser 602 respectively (Figures 1d and 1e). These bound too weakly for reliable affinity measurement by bioassay, as observed previously for fragment hits against "challenging" targets, which often require sensitive biophysical techniques such as X-ray crystallography for their detection[40]. Nevertheless, the potency of such hits can often be rapidly optimized by structure-based design to bring them "on-scale", and the phenyl acetic acid fragment **1** in particular was identified as a promising "anchor fragment" for hit elaboration as discussed below.

Mimicking Glu 79 of the NRF2 ETGE motif, the carboxylic acid of **1** is engaged in a key electrostatic interaction with Arg 483 on the KEAP1 Kelch domain (Figure 1f). It was known from mutagenesis of NRF2 that electrostatic interactions with positively charged residues in the Arg 483 region are important for binding[27], and an acidic moiety as exemplified in fragment **1** was anticipated to be required for potent activity in a lead molecule. Despite its low potency (IC_{50} >1 mM; Table 1), inspection of the complex structure suggested that **1** also had exit vectors which would be well suited for fragment growing. For example, growth from the benzylic carbon would allow interaction with the hot-spot occupied by fragment **2**, whilst growth from the phenyl ring, *ortho* to the chlorine, would allow access to the subsite identified by the sulphonamide fragment **3**. In addition, fragment binding elicited a conformational change in the side chain of Arg 415 relative to apo and peptide-bound Kelch structures,[24] creating an enclosed and potentially more drugable interaction surface within the NRF2 pocket (Figure 1g).

This hit was subsequently modified in a step-wise manner to fill the remainder of the NRF2 site in a structure-driven approach (Figure 2a), with potency assessed using both a fluorescence polarization (FP) assay, and isothermal scanning calorimetry (ITC) (Table 1). We sought where possible to exploit information provided by the ensemble of fragment hits, which provided a direct insight into the minimal pharmacophore required for potent binding to the pocket.

The benzotriazole moiety was chosen for attachment directly to the benzylic carbon of the phenyl acetic acid, supported by docking studies which suggested it could form a stacking interaction with the side-chain Tyr 525 whilst also satisfying the hydrogen bonding requirements of both Gln 530 and Ser 555 with a bidentate acceptor motif. This initial modification gave a sufficient increase in affinity to allow detection using the FP assay and ITC (IC_{50} = 61 μM; ITC K_d = 59 μM). The co-structure of compound **4** with KEAP1 shows that the benzotriazole

interacts with KEAP1 as predicted, and recapitulates the molecular recognition displayed by the "aromatic-acceptor" fragment **2** (Figure 2a). Similarly, comparison of the KEAP1-**4** structure with that for sulfonamide fragment **3** suggested that growth from the 3-position of the chlorophenyl ring of **4** with a sulfonamide group could reproduce the fragment's hydrogen bonding interaction with Ser 602. This was observed to be the case (compound **5**, Figure 2b), and resulted in a further 18-fold increase in affinity (IC_{50} = 3.4 μM). Introduction of the sulfonamide at this position was also observed to provide a useful exit vector with which to introduce aromatic functionality to exploit the lipophilic edge of the pocket by π-stacking with Tyr 334 (Figure 2c), as exemplified by compound **6** which exhibited sub-micromolar potency (IC_{50} = 0.27 μM). Throughout this optimization process there were only small perturbations of the binding mode relative to the initial fragment hit, and good overlay of the iteratively introduced pharmacophore elements such as the benzotriazole, suggesting well optimized interactions with the NRF2-binding pocket (Figure 2c). The protein structure also displayed only modest adjustments during the fragment elaboration, with the exception of Arg 415 which was observed to adopt an alternative rotamer when bound to the *meta*-substituted compounds **5** and **6**.

A number of small, structure-driven modifications to compound **6** were then made to afford further gains in potency. Replacement of the *para*-chloro-phenyl with methyl was anticipated to relieve potentially unfavourable intramolecular contacts with the sulfonamide centre, whilst an electron donating methoxy group was introduced at the benzotriazole 7-position to increase the hydrogen bond accepting potential of the ring nitrogens and add additional surface contacts. Cyclization of the phenyl sulphonamide to form the fused 7-membered benzoxathiazepine was introduced to rigidify the molecule in its bound conformation, and provided additional vectors to fill the space between the sulphonamide and benzotriazole moieties. Although compounds **4** – **6**

were prepared and soaked as the racemates, only the (*S*) enantiomers were observed to bind by crystallography. The combination of the modifications to the initial fragment described above, and the observation of this stereoselective binding led to the identification of **7** (Table 1; Figures 2d and 2e). This compound fulfils the three-point pharmacophore identified from the fragment screen (acid, aromatic-acceptor and sulfonamide) and exhibits very high affinity for the KEAP1 Kelch domain (ITC K_d = 1.3 nM, Figure 2f).

To assess its selectivity towards the Kelch domain of KEAP1, compound **7** was screened against GSK's Enhanced Cross-screen Panel (eXP),[41] which consists of 49 *in vitro* functional assays for targets which may represent toxicity liabilities. With the exception of the organic anion transporting polypeptide 1B1 (OATP1B1) (IC_{50} = 2.5 μM), the bile salt export pump BSEP (IC_{50} = 4.0 μM), and the phosphodiesterase PDE3A (IC_{50} = 10 μM), no significant cross-reactivity was observed (see supplemental Table S1). No cytotoxicity was observed towards BEAS-2B cells with compound **7** at concentrations up to 10 μM (cell titer glo assay). We therefore believe that compound **7** possesses a suitable selectivity profile as a tool compound for cell-based and *in vivo* studies.

Comparison of NRF2 and compound 7 binding to the KEAP1 Kelch domain

To compare the interactions between compound **7** and KEAP1 with those formed by the tight binding ETGE motif of NRF2, we overlaid Kelch-bound structures of the lead compound with that for a fragment of NRF2 (Leu 76–Leu 84; sequence LDEETGEFL) containing the ETGE sequence embedded within a 9-mer β-turn (PDB 1x2r[24]; Figure 3a). A key observation from this is that compound **7** is not a peptidomimetic, with little overlap between its binding footprint and

that of NRF2. Nevertheless a careful analysis does reveal a conservation of key pharmacophore points, as described below.

As evident from the fragment hit, the main point of similarity with the natural ligand is the carboxylic acid of compound **7**, which occupies a similar region of space to Glu 79 of NRF2 (Figure 3b), both of which form electrostatic interactions with the basic side-chain of Arg 483. As mentioned earlier, mutational analysis of NRF2 had previously demonstrated the importance of Glu 79 for tight binding[27], and our data confirm the presence of this key hot-spot in the Kelch-NRF2 interface. In addition, stacking interactions of the planar peptide backbone between Glu 78 and Glu 79 are partially mimicked by the benzotriazole ring, and there is a good overlay of the peptide carbonyl oxygen and the N2 benzotriazole nitrogen, both of which accept a hydrogen bond from the side-chain of Gln 530 (Figure 3c). The potential to build potency by interaction with this region was evident from the fragment screen with a number of small aromatic heterocycles (eg **2**) observed to bind here. Away from these regions, the interactions formed by the lead and ETGE peptide diverge. Although the phenyl-sulfonamide of compound **7** occupies a region of the pocket broadly similar to the NRF2 Glu 82 side-chain, and both exploit a hydrophobic stack with Tyr 334, the electrostatic interaction formed between Arg 380 and NRF2 Glu 82 is not present for our lead. This result, which is consistent with the detection of the uncharged sulphonamide fragment **3**, highlights that a second acidic moiety at this position is not required for potency if other interactions are efficiently optimized. Similar to the chloro-phenyl in the fragment hit, the tolyl group of the lead occupies a region of the pocket at the entrance to the central tunnel which is unexploited by the ETGE peptide, and leads to a change in rotamer of Arg 415.

Much of the remainder of the ETGE-containing turn makes little contact with the protein, and presumably provides a scaffold to pre-form a globular architecture complementary to the bowl of the KEAP1 pocket whilst rigidly orientating the glutamate residues in an optimal position. By contrast, compound **7** fills the pocket more efficiently, with a much larger proportion forming direct interactions with the NRF2 site (Figure 3d). The result is that **7** (MW = 551) exhibits higher affinity and efficiency in binding compared with much larger and more hydrophillic NRF2-derived peptides (e.g., Leu 76-Leu 84 (Figure 3a); K_d = 182 nM;[26] MW = 1052), resulting in a compound with physicochemical properties that are suitable for progression to cell-based and *in vivo* studies. Of particular note is that compound **7** contains only a single carboxylic acid functionality, compared with five in the Leu 76-Leu 84 peptide.

Assessment of compound 7 in cellular and in vivo models

Chronic obstructive pulmonary disease (COPD) is a disease associated with excessive levels of electrophilic stress and inflammation, and activation of the KEAP1/NRF2 pathway by covalent modification of KEAP1 cysteine residues has been shown to reduce cigarette smoke-induced emphysema (a key feature of COPD) in an NRF2-dependent fashion in mice.[21,42,43] An assessment in cellular and *in vivo* models of relevance to this disease area therefore provides an opportunity to assess the pharmacological effects and therapeutic relevance of disrupting the Kelch-NRF2 interaction, and allows comparison with covalent activators of the NRF2 pathway. Multiple sources of human lung epithelial cells were treated with compound **7** to gain an understanding of pathway activation *in vitro*, followed by *in vivo* studies with Han Wistar rats.

Compound 7 increases NRF2 Nuclear Translocation in Normal Human Bronchial Epithelial cells

To assess whether disruption of the Kelch-NRF2 interaction by compound **7** can increase levels of NRF2 in a cellular context, we firstly measured the amount of nuclear NRF2 protein accumulation in Normal Human Bronchial Epithelial (NHBE) cells. Cells were treated with compounds or DMSO vehicle for 6 hours, after which cytoplasmic and nuclear fractions were generated for assessment of NRF2 protein levels. Compound **7** increased the accumulation of nuclear NRF2 protein in a concentration-dependent manner (supplemental Figure S1). The commercially available NRF2 activators tert-butylhydroquinone (tBHQ) and CDDO-Me were included as positive controls.

Compound 7 up-regulates NRF2-dependent gene expression

We next assessed the ability of compound **7** to upregulate NRF2-dependent gene expression in human primary lung epithelial cells. NHBE cells were transfected with 25 nM non-targeting or *NRF2* siRNA for 48 hours followed by 24 hours treatment with DMSO, compound **7**, or CDDO-Me, which activates NRF2 through covalent modification of KEAP1 BTB. Compound **7** increased mRNA expression of the NRF2-dependent genes *NQO1* and *GCLM* in NHBE cells transfected with the non-targeting siRNA, while *NRF2* gene silencing significantly decreased compound activity (Figure 4a). Similar results were seen in cells treated with CDDO-Me. Confirmation that *NRF2* siRNA treatment effectively decreases *NRF2* mRNA expression is shown in supplemental Figure S2.

Compound 7 increased NQO1 Activity in an NRF2-Dependent Manner

To confirm that compound **7** activated NRF2 and led to the induction of the NRF2-dependent downstream signalling cascade, we measured the ability of **7** to increase NQO1 enzyme activity. NHBE cells were transfected with *NRF2* or non-targeting siRNA for 48 hours before treatment with DMSO, 100 nM CDDO-Me, or 1 μM compound **7** for another 48 hours. NQO1 specific enzyme activity was then assayed in crude cell lysates. Figure 4b shows that compound **7** induced NQO1 specific enzyme activity by 6-fold over the DMSO control and *NRF2* siRNA abolished approximately 88% of the activity above vehicle-treated, non-targeting siRNA levels. Similar NRF2-dependent activity was seen in cells treated with CDDO-Me. The ability of **7** to increase NQO1 activity was also confirmed in a human lung epithelial cell line, BEAS-2B, with an EC_{50} of 12 nM (Fig 4c).

Compound 7 prevents tBHP-induced glutathione depletion

The *in vitro* functional activity and cytoprotective effects of compound **7** were next assessed in response to oxidative stress. NHBE cells were pre-treated with compounds or DMSO for approximately 18 hours before addition of 300 μM tert-butyl hydroperoxide (tBHP), an oxidative stress agent that causes rapid oxidation of reduced glutathione (GSH) and other events that decrease cell viability.[44] As shown in Figure 4d, treatment with 300 μM tBHP decreased GSH levels by approximately 63% compared to the media control. The γ-glutamylcysteine synthetase inhibitor buthionine sulfoxide (BSO) and glutathione precursor N-acetyl cysteine (NAC) were used as internal controls. The application of 1 mM NAC increased total glutathione levels approximately 4-fold over media alone, whereas 3 mM BSO decreased glutathione content by

approximately 37%. Pre-treatment with NAC or the NRF2-activating compound CDDO-Me prevented tBHP-induced glutathione depletion. The Kelch targeting compound **7** increased intracellular glutathione levels in a concentration-dependent manner. In addition, morphological changes were also examined in NHBE cells with DMSO, tBHP, or compound **7** + tBHP treatment. Treatment with tBHP clearly had a detrimental effect on cell health and appearance while pre-treatment of cells with 1 μM compound **7** before the exposure to tBHP maintained cell morphology consistent with the DMSO control (supplemental Figure S3).

Compound 7 Induces the Expression of NRF2-Regulated Genes in COPD patient-derived bronchial epithelial cells

We next evaluated the ability of compound **7** to up-regulate NRF2-dependent gene expression in human disease-derived cells. Bronchial epithelial cells from human COPD patient lung brushings were grown and differentiated into air-liquid interface (ALI) culture conditions. ALI cells were treated for 6 hrs with compound **7** and expression of NRF2-dependent genes, including *NQO1*, *TXNRD1*, *GCLM* and *HO-1* was measured using real-time PCR. As shown in Figure 4e, compound **7** efficiently up-regulated expression of each of these genes in a concentration-dependent manner. The EC_{50} obtained for *NQO1* mRNA expression in the lung brushing cells correlates closely with the EC_{50} observed with the NQO1 activity assay in BEAS-2B cells (22 nM and 12 nM, respectively). These data demonstrate the ability of compound **7** to upregulate NRF2 signalling not only in healthy cells as previously shown, but also in a translational model of human disease.

Compound 7 Induces the Pulmonary Expression of NRF2-Regulated Genes in vivo

In order to study the *in vivo* effects of compound **7**, IV and oral pharmacokinetic parameters were determined (Figure S4). A relatively high clearance and short half-life were observed after IV dosing, with low oral bioavailability (F = 7%). Hence, IV infusions were used in order to achieve sustained target engagement when studying the *in vivo* pharmacology of compound **7**. To confirm engagement of the NRF2 pathway by compound **7** *in vivo*, Han Wistar rats were administered the compound by IV infusion over 6 hours, and lung tissue was analyzed for expression of the NRF2-regulated genes *Nqo1*, *Ho-1*, *Txnrd1*, *Srxn1*, *Gsta3* and *Gclc*. As shown in Figure 5a, compound **7** induced the expression of each of the 6 genes in a dose-dependent manner, with maximum increases over vehicle controls of 37- (*Nqo1*), 17- (*Ho-1*), 9-(*Txnrd1*), 28- (*Srxn1*), 15- (*Gsta3*) and 13-fold (*Gclc*) occurring at the 50 μmol/kg dose. EC_{50} values were 44.0, 25.7, 42.6, 33.8, 28.4, and 44.1 μmol/kg, respectively, giving an average EC_{50} value of 36.4 $\pm$ 3.4 μmol/kg.

Compound 7 Attenuates Ozone-Induced Pulmonary Inflammation in vivo

To examine the effect of compound **7** under conditions of oxidative stress, rats were administered the compound at 35 μmol/kg (the approximate average EC_{50} value for gene expression) by IV infusion over 6 hours, and after 24 hours were exposed to ozone (1 ppm for 3 hours). Fifteen minutes following the termination of ozone exposure, the numbers of total cells, neutrophils and mononuclear cells in the bronchoalveolar lavage (BAL) fluid were significantly increased in vehicle-treated ozone-exposed rats compared to vehicle-treated air-exposed rats

(Figure 5b). The ozone-induced increase in each cell subset was significantly reduced as a result of compound **7** treatment.

Compound 7 Restores Ozone-Induced Depletion of Lung GSH Levels in vivo

In a subsequent study, compound **7** was administered to rats at 10, 35 and 50 μmol/kg by IV infusion, resulting in steady state compound concentrations in the blood of 407 ± 44 nM, 946 ± 50 nM and 1437 ± 186 nM, respectively, over the 6 hour infusion period. Exposure to ozone 24 hours post-dose produced a significant depletion in lung levels of the anti-oxidant molecule, GSH, which was restored by compound **7** in a dose-dependent manner (Figure 5c).

Synthesis

Fragments **1** - **3** were purchased from commercial sources. The propionic acid **4** was synthesized according to Scheme 1. Addition of 4-chlorophenylmagnesium bromide to the benzotriazolyl aldehyde **10** gave the carbinol **11**, which was oxidized to the ketone **12** using Dess-Martin periodinane. The carboxy side chain was then introduced by a Horner-Wadsworth-Emmons condensation with ketone **12** followed by reduction with nickel borohydride and *in situ* saponification to give acid **4** in four steps overall.

The methanesulfonamide-substituted aryl propionic acid **5** was prepared according to Scheme 2. First, the N-methyl methanesulfonamide group was introduced by displacement of the benzylic bromide **14**. Next, Horner-Wadsworth-Emmons condensation gave the cinnamate ester **16**,

which allowed rhodium-catalysed conjugate addition of the boronate ester **18** to give, after saponification, the acid **5** in five steps overall.

The benzenesulfonamide **6** was prepared using an analogous, but complementary route (Scheme 3). Horner-Wadsworth-Emmons condensation with the benzotriazolyl aldehyde **10** gave the cinnamate ester **19**, which was subjected to rhodium-catalysed conjugate addition of 4-chloro-3-hydroxymethylphenyl pinacol boronate ester to give the intermediate bisaryl propionate **20**, containing a hydroxymethyl group as a handle for further derivatisation. Displacement of the hydroxyl group with N-methyl benzenesulfonamide under Mitsunobu conditions followed by chiral HPLC gave the (*S*)-methyl ester **21**, which was saponified to give the acid **6** in five steps overall.

The benzoxathiazepine **7** was prepared according to Scheme 4. This required the synthesis of the 5-bromo-1-methyl-7-methoxybenzotriazole intermediate **7**. Starting from 2-amino-3-nitrophenol (**22**), selective O-methylation followed by bromination under acidic conditions gave anisole **24**, which was N-methylated and then reduced to give the diaminoanisole **26**. Diazotization with sodium nitrite then gave the benzotriazole **27**. This was converted to the cinnamate ester **28** by Heck coupling, allowing rhodium-catalysed conjugate addition of 4-chloro-3-hydroxymethylphenyl pinacol boronate ester to give the intermediate bisaryl propionate **29**. The key benzoxathiazepine intermediate **32** was prepared by sulfonylation of (*R*)-1-aminopropanol (**30**) with 2-fluorobenzenesulfonamide followed by cyclization under basic conditions. Coupling of the two intermediates **29** and **32** under Mitsunobu conditions followed by saponification and chiral HPLC gave the desired stereoisomer **7** in a total of 12 steps.

DISCUSSION

We have described here the successful identification of compound **7**, a highly potent and selective inhibitor of the KEAP1 Kelch-NRF2 interaction with the ability to stimulate the NRF2 pathway in both human cell-based assays, and *in vivo*. KEAP1 is increasingly recognized as a key node for therapeutic intervention in a range of diseases involving chronic oxidative stress, including respiratory and cardiovascular indications, diabetic nephropathy and neurodegeneration. Indeed, the approved multiple sclerosis drug Tecfidera is a NRF2 activator, and is believed to operate at least in part through this mechanism of action.[23] However, compounds that have so far been progressed to clinical trials lack selectivity due to their electrophilic mode of action, and this may lead to pleiotropic effects. For example, an analogue of the widely studied NRF2 inducer CDDO has been shown to react with over 500 molecular species,[45] and the therapeutic outcome of such compounds is likely to result from activities against multiple targets. The inherent lack of selectivity observed for this class of compound may lead to a low therapeutic index, but also hinders attempts to clearly dissect and understand the consequences of pharmacological activation of NRF2. By contrast, non-covalent disruption of the Kelch-NRF2 interaction is likely to afford the opportunity for more specific modulation of this pathway.

Although a number of small-molecule inhibitors of the KEAP1 Kelch-NRF2 interaction have recently been identified, an important aspect of this work was the use of a fragment-based approach which allowed the development of a novel, non-peptidomimetic inhibitor that combines high potency with more drug-like physicochemical properties. For example, the fragment screen highlighted the ability of non-charged moieties to bind close to the region occupied by the NRF2 Glu 82 side-chain, and we have shown here that a single acidic

functionality is sufficient to achieve highly potent binding in an elaborated compound. This detailed understanding of the KEAP1 Kelch pharmacophore afforded by the fragment screen, together with a parsimonious fragments to leads design approach, allowed the progression from a hit with >1 mM potency to a nanomolar lead compound which was well suited for biological evaluation.

Compound **7** showed benefit in both cell and animal models of oxidative stress-induced respiratory disease. Compound **7** induced the expression of NRF2-regulated genes such as *NQO1*, as well as the corresponding NQO1 enzyme activity, in normal human bronchial epithelial cells. The inhibition of these inductions in cells treated with NRF2-targeting siRNA, but not with non-targeting siRNA, confirms that compound **7** exerts these effects through NRF2. Similar induction of NRF2-regulated gene expression was observed in the lungs of compound **7**-treated rats, demonstrating compound activity *in vivo*. Importantly, compound **7**-induced gene expression was also observed in bronchial epithelial cells derived from COPD patients, providing a translational link to the human disease state.

GSH is a molecule that plays a crucial role in protecting cells from oxidative damage, leading to the pursuit of therapeutic strategies that modulate GSH content. In both our *in vitro* and *in vivo* models, exposure to oxidants such as tBHP and ozone resulted in decreases in GSH content, which were restored in a dose-dependent manner by compound **7**. *In vivo* ozone exposure also induces the influx of inflammatory cells into the lungs, allowing for examination of the anti-inflammatory effects of potential therapeutics. Here we demonstrate that the ozone induces increases in BAL fluid total cells, neutrophils and mononuclear cells that can be significantly inhibited by compound **7**.

Collectively, these studies provide consistent evidence across human cell-based and *in vivo* models that compound **7** activates the NRF2 pathway, resulting in induction of target gene expression and downstream anti-oxidant and anti-inflammatory activities. To the best of our knowledge, compound **7** represents the most potent small-molecule KEAP1-NRF2 inhibitor so far reported, and the demonstration of its high selectivity and detailed mode of action studies both *in vitro* and *in vivo* allow its observed phenotypic effects to be confidently related to on-target activity. In fulfilling these criteria, compound **7** provides an important new chemical probe with which to further study the biology of the KEAP1/NRF2 axis, and represents a promising lead compound for diseases where maladaptive NRF2 pathway activation is implicated.

EXPERIMENTAL PROCEDURES

*Synthesis of Compounds **4-7***

All solvents and commercially available reagents were used as received. All reactions were followed by TLC analysis (TLC plates GF254, Merck) or LC-MS (liquid chromatography mass spectrometry). LC-MS analysis was performed with an Agilent or Shimadzu LC system with variable wavelength UV detection using reverse phase chromatography with a CH_3CN and water gradient with a 0.02 or 0.1% TFA modifier (added to each solvent) and using a reverse phase column, e.g., Thermo Hypersil Gold C18. MS was determined using either PE Sciex 150EX LC-MS, Waters ZQ LC-MS, or Agilent 6140 LC-MS Single Quadrupole instruments. Column chromatography was performed on prepacked silica gel columns (3090 mesh, IST) using a Biotage SP4 or similar. NMR spectra are referenced as follows: ^1H (400 MHz), internal standard TMS at $\delta = 0.00$. Abbreviations for multiplicities observed in NMR spectra: s; singlet; br s, broad singlet; d, doublet; t, triplet; q, quadruplet; p, pentuplet; spt, septuplet; m, multiplet. All compounds reported are of at least 95% purity according to LC-MS unless stated otherwise.

3-(4-Chlorophenyl)-3-(1-methyl-1H-1,2,3-benzotriazol-5-yl) propanoic acid (4)

A stirred solution of t-BuOK (0.372 g, 3.31 mmol) in THF (22 mL) at 0°C under N_2 was treated with trimethyl phosphonoacetate (0.903 g, 4.86 mmol). After 10 mins, 5-(4-chlorobenzoyl)-1-methyl-1H-1,2,3-benzotriazole (0.600 g, 2.21 mmol) was added slowly. The mixture was allowed to warm to ambient temperature and then stirred for 72 h. The mixture was quenched with NH_4Cl (aq., sat.), diluted with water and then extracted with n-heptane (x3). The combined organic layers were washed with water and brine, dried over $MgSO_4$, filtered and concentrated to

dryness to give a colourless solid, used without further purification (640 mg, 88%). LC-MS $[M+H]^+$ 328/330 (Cl), rt 1.40/1.43 min (2 isomers). A stirred solution of this material (0.640 g, 1.95 mmol) in MeOH (20 mL) under N_2 was treated with $NiCl_2.6H_2O$ (0.093 g, 0.39 mmol), then cooled to 0°C and treated with $NaBH_4$ (0.222 g, 5.86 mmol) slowly in portions. The mixture was allowed to warm to ambient temperature and stirred for 4 h, then treated with NaOH (2M, 40 mL) and stirred overnight. The mixture was then quenched with NH_4Cl (sat., aq.) and extracted with EtOAc. The organic layer was dried over $MgSO_4$, filtered and concentrated under reduced pressure. The residue was purified by phenomenix silica cartridges by gradient elution (100% DCM to 50 % EtOAc in DCM) to give the product as a buff solid (0.307 g, 50%). LC-MS $[M+H]^+$ 316/318 (Cl), rt 1.24 min. ^{1}H NMR (400 MHz, Me-d_3-OD): 7.92 (s, 1H), 7.68 (d, 1H), 7.49 (dd, 1H), 7.38-7.26 (m, 4H), 4.73 (t, 1H), 4.31 (s, 3H), 3.23-3.10 (m, 2H).

3-{4-Chloro-3-[(N-methylmethanesulfonamido)methyl]phenyl}-3-(1-methyl-1H-1,2,3-benzotriazol-5-yl)propanoic acid (5)

A stirred mixture of 5-bromo-1-methylbenzotriazole (prepared according to PCT Int. Appl., 2012119046; 1.28 g, 6.04 mmol), bis(pinacolato)diboron (1.69 g, 6.04 mmol), KOAc (1.18 g, 12.08 mmol) and $PdCl_2$dppf (0.221 g, 0.30 mmol) in dioxane was degassed with N_2 for 10 mins and then heated at 90°C for 5 hours. After cooling the mixture was partitioned between water and EtOAc. The organic phase was dried ($MgSO_4$), filtered and concentrated to dryness. The residue was purified by flash chromatography (EtOAc/petrol gradient 0-40%) to give 1-methyl-5-(4,4,5,5-tetramethyl-[1,3,2]dioxaborolan-2-yl)-1H-benzotriazole (1.21 g, 72%). LC-MS $[M+H]^+$ 260, rt 1.30 min. A stirred mixture of this material (0.191 g, 0.74 mmol), (*E*)-3-{4-

chloro-3-[(methanesulfonyl-methyl-amino)-methyl]-phenyl}-acrylic acid methyl ester (0.117 g, 0.37 mmol), $[RhCl(cod)]_2$ (0.009 g, 0.02 mmol), triethylamine (0.056 g, 0.55 mmol), 1,4-dioxane (0.18 mL) and water (1.23 mL) was heated in a reactivial at 95°C for 18 hours. LiOH (1M, 2 mL) was added and the mixture stirred at ambient temperature for 2 hours. The mixture was treated with citric acid (5%, aq.) and extracted with $CHCl_3$:IPA (3:1, x2). The combined organic layers were washed successively with water and brine, dried over $MgSO_4$, filtered and concentrated to dryness. Purification by preparative HPLC (Agilent, formic acid method and Agilent TFA) gave the product as a colourless oil (0.028 g, 17%). LC-MS $[M+H]^+$ 437/439 (Cl), rt 0.99 min. ^{1}H NMR (400 MHz, Me-d_3-OD): 7.92 (s, 1H), 7.69 (d, 1H), 7.56-7.46 (m, 2H), 7.37 (d, 1H), 7.29 (dd, 1H), 4.75 (t, 1H), 4.44 (s, 2H), 4.31 (s, 3H), 3.18 (d, 2H), 2.92 (s, 3H), 2.76 (s, 3H).

(3*S*)-3-{4-Chloro-3-[(N-methylbenzenesulfonamido)methyl]phenyl}-3-(1-methyl-1H-1,2,3-benzotriazol-5-yl)propanoic acid (6)

A stirred solution of (*S*)-methyl 3-(4-chloro-3-((N-methylphenylsulfonamido) methyl)phenyl)-3-(1-methyl-1H-benzo[d][1,2,3]triazol-5-yl)propanoate (0.180 g, 0.351 mmol) in methanol (15 mL) and THF (1 mL) at ambient temperature was treated with a 1M solution of lithium hydroxide (16 mL, 16.00 mmol). The resulting suspension was diluted with methanol (10 mL). After 1 hr 20 mins at ambient temperature the reaction mixture was acidified to pH 1-2 and the solution diluted with ethyl acetate. The organic phase was washed with water (2x), dried over magnesium sulfate, filtered, and concentrated to give 0.156 g of a light yellow solid. This material was dissolved in chloroform and concentrated (3x) to give 0.141 g of the title compound

as a light yellow solid. LC-MS $[M+H]^+$ 499/501 (Cl), rt 1.03 min. ^{1}H NMR (400 MHz, methanol-d_4) δ 7.83 - 7.90 (m, 3H), 7.59 - 7.71 (m, 4H), 7.46 (d, J=8.8 Hz, 1H), 7.39 (s, 1H), 7.30 - 7.34 (m, 1H), 7.24 - 7.28 (m, 1H), 4.70 (t, J=8.2 Hz, 1H), 4.28 - 4.33 (m, 5H), 3.12 (dd, J=7.8, 3.8 Hz, 2H), 2.61 (s, 3H).

(3*S*)-3-(7-Methoxy-1-methyl-1H-benzo[d][1,2,3]triazol-5-yl)-3-(4-methyl-3-(((*R*)-4-methyl-1,1-dioxido-3,4-dihydro-2H-benzo[b][1,4,5]oxathiazepin-2-yl)methyl)phenyl)propanoic acid (7)

To a solution of ethyl 3-(3-(hydroxymethyl)-4-methylphenyl)-3-(7-methoxy-1-methyl-1H-benzo[d][1,2,3]triazol-5-yl)propanoate (980 mg, 2.56 mmol) in THF (30 mL) was added (*R*)-4-methyl-3,4-dihydro-2H-benzo[b][1,4,5]oxathiazepine 1,1-dioxide (818 mg, 3.83 mmol), PS-PPh_3 (3195 mg, 5.11 mmol) and then was added diisopropyl azodicarboxylate (DIAD) (0.994 mL, 5.11 mmol) in tetrahydrofuran (THF) (10 mL). The resulting reaction mixture was stirred at room temperature for 30 min. The reaction mixture was filtered and the filtrate was concentrated under reduced pressure, purified with flash chromatography over silica gel column to afford desired crude intermediate ethyl 3-(7-methoxy-1-methyl-1H-benzo[d][1,2,3]triazol-5-yl)-3-(4-methyl-3-(((*R*)-4-methyl-1,1-dioxido-3,4-dihydro-2H-benzo[b][1,4,5]oxathiazepin-2-yl)methyl)phenyl)propanoate (1.30 g, 88%). This crude intermediate was dissolved in methanol (30.0 mL) then was added NaOH (2 N, 6.39 mL, 12.8 mmol). The resulting reaction mixture was stirred at 80ºC for 40 min. The reaction mixture was acidified with HCl (1 N) to pH ~3, concentrated under reduced pressure, extracted with EtOAc (3 x 50 mL). The combined organic layers were washed with brine (50 mL), dried over $MgSO_4$, filtered, and concentrated under reduced pressure to afford the desired product 3-(7-methoxy-1-methyl-1H-

benzo[d][1,2,3]triazol-5-yl)-3-(4-methyl-3-(((*R*)-4-methyl-1,1dioxido-3,4-dihydro-2H-benzo[b][1,4,5]oxathiazepin-2-yl)methyl)phenyl)propanoic acid (1.41 g, 100%). The title compound was obtained by SFC chiral purification to afford the desired enantiomerically pure product (0.367 g, 26%). LC-MS $[M+H]^+$ 551, rt 1.02 min. ^{1}H NMR (400 MHz, DMSO-d_6) δ 1.11 (d, J=6.27 Hz, 3 H), 2.24 (s, 3 H), 2.76 (d, J=15.06 Hz, 1 H), 3.06 - 3.16 (m, 2 H), 3.62 (dd, J=15.31, 10.29 Hz, 1 H), 3.82 (d, J=14.05 Hz, 1 H), 3.94 (s, 3 H), 4.34 - 4.47 (m, 6 H), 4.51 (t, J=7.78 Hz, 1 H), 6.93 (s, 1 H), 7.12 (d, J=7.78 Hz, 1 H), 7.28 - 7.32 (m, 2 H), 7.36 - 7.38 (m, 2 H), 7.45 (s, 1 H), 7.66 (t, J=7.65 Hz, 1 H), 7.78 (d, J=7.53 Hz, 1 H), 12.08 (br s, 1 H). The ^{1}H NMR spectrum for compound **7** is given in Supplemental Figure S5.

(4-Chlorophenyl)(1-methyl-1H-1,2,3-benzotriazol-5-yl)methanol (11)

A stirred solution of 1-methyl-1H-1,2,3-benzotriazole-5-carbaldehyde (0.500 g, 3.10 mmol) in THF at 0°C under N_2 was treated with a solution of 4-chlorophenylmagnesium bromide in THF (1M, 3.72 mL, 3.72 mmol). After 2 hours the mixture was quenched with NH_4Cl (sat., aq.) and warmed to ambient temperature. The mixture was extracted with DCM (x3) and the combined organic layers were washed with water followed by brine, dried over $MgSO_4$, filtered and concentrated to dryness to give a yellow solid, used without further purification (0.800 mg, 94%). LC-MS $[M+H]^+$ 274/276 (Cl), rt 1.23 min. ^{1}H NMR (400 MHz, DMSO-d_6): 8.03 (s, 1H), 7.75 (d, 1H), 7.49 (dd, 1H), 7.43 (d, 2H), 7.36 (d, 2H), 6.15 (d, 1H), 5.91 (d, 1H), 4.27 (s, 3H).

5-(4-Chlorobenzoyl)-1-methyl-1H-1,2,3-benzotriazole (12)

A solution of (4-chlorophenyl)(1-methyl-1H-1,2,3-benzotriazol-5-yl)methanol (0.800 g, 2.92 mmol) in dichloromethane (29 mL) was treated with Dess-Martin periodinane (1.49 g, 3.51 mmol) at 0°C, under N_2. After stirring for 1 h at ambient temperature, the reaction mixture was diluted with sodium bicarbonate (sat., aq.) and extracted with $CHCl_3$ (x3). The combined organic layers were washed with water followed by brine, dried over $MgSO_4$, filtered and concentrated to dryness to leave a yellow solid. This was purified by phenomenix silica cartridge (100% $CHCl_3$) and the residue was washed with a small amount of MeOH to yield a colourless solid (600 mg, 76%). LC-MS $[M+H]^+$ 272/274 (Cl), rt 1.36 min. ^{1}H NMR (400 MHz, DMSO-d_6): 8.37 (s, 1H), 8.04 (s, 1H), 7.98 (dd, 1H), 7.82 (d, 2H), 7.67 (d, 2H), 4.39 (s, 3H).

(*E*)-3-{4-Chloro-3-[(methanesulfonyl-methyl-amino)-methyl]-phenyl}-acrylic acid methyl ester (16)

A mixture of 4-chloro-3-(bromomethyl)benzaldehyde (0.25g, 1.07 mmol), N-methyl methanesulfonamide (0.129g, 1.18 mmol) and K_2CO_3 (0.163g, 1.18 mmol) in MeCN was stirred at ambient temperature under N_2 overnight. The mixture was diluted with water and extracted with DCM (x3). The combined organic layers were washed with brine and dried over $MgSO_4$. Filtration and concentration to dryness afforded N-(2-chloro-5-formyl-benzyl)-N-methyl-methanesulfonamide as a yellow oil (0.247g, 88%), used without further purification. LC-MS $[M+18]^+$ 279/281 (Cl isotopes), rt 1.15 min. A stirred solution of *t*-BuOK (0.212g, 1.89 mmol) in THF (10 mL) at 0°C under N_2 was treated with trimethyl phosphonoacetate (0.403g, 2.17 mmol). After 30 mins, a solution of N-(2-chloro-5-formyl-benzyl)-N-methyl-methanesulfonamide (0.247g, 0.94 mmol) in THF (2 mL) was added. The mixture was stirred for 3 hours, then treated

with NH_4Cl (aq., sat.), diluted with water and extracted with DCM (x3). The combined organic layers were washed with water and brine and dried over $MgSO_4$. Filtration and concentration to dryness followed by purification by silica gel chromatography (100% DCM) gave the product as a colourless solid (0.277g, 92%). LC-MS $[M+H]^+$ 335/337 (Cl), rt 1.30 min. ^{1}H NMR (400 MHz, Me-d_3-OD): 7.75 (d, 1H), 7.71 (d, 1H), 7.59 (dd, 1H), 7.50 (d, 1H), 6.58 (d, 1H), 4.50 (s, 2H), 3.81 (s, 3H), 3.01 (s, 3H), 2.85 (s, 3H).

(*E*)-Methyl 3-(1-methyl-1H-benzo[d][1,2,3]triazol-5-yl)acrylate (19)

A stirred suspension of potassium *tert*-butoxide (108 mg, 0.96 mmol) in THF (4 mL) at 0°C was treated with methyl 2-(dimethoxyphosphoryl)acetate (0.18 mL, 1.12 mmol) in THF (4 mL). The reaction mixture was stirred at 0°C for 1.5 h. Then 1-methyl-1H-benzo[d][1,2,3] triazole-5-carbaldehyde (100 mg, 0.62 mmol) was added in one portion. The suspension was stirred at 0ºC for 1.5 h. The reaction was quenched via addition of saturated ammonium chloride solution and diluted with water. A precipitate formed which was filtered and dried to give the title compound (105 mg, 78%). LC-MS $[M+H]^+$ 218.0, rt 0.68 min. ^{1}H NMR (400 MHz, chloroform-*d*) δ 8.18 (s, 1H), 7.86 (d, J=16.1 Hz, 1H), 7.72 (dd, J=8.7, 1.4 Hz, 1H), 7.53 (d, J=8.8 Hz, 1H), 6.52 (d, J=15.8 Hz, 1H), 4.32 (s, 3H), 3.84 (s, 3H).

Methyl 3-(4-chloro-3-(hydroxymethyl)phenyl)-3-(1-methyl-1H-benzo[d][1,2,3]triazol-5-yl)propanoate (20)

A stirred suspension of (2-chloro-5-(4,4,5,5-tetramethyl-1,3,2-dioxaborolan-2-yl)phenyl) methanol (500 mg, 1.86 mmol), (*E*)-methyl 3-(1-methyl-1H-benzo[d][1,2,3]triazol-5-yl)acrylate

(640 mg, 2.95 mmol) and chloro(1,5-cyclooctadiene)rhodium(I) dimer (92 mg, 0.19 mmol) in water (8 mL) and 1,4-dioxane (1.5 mL) at room temperature was treated with triethylamine (0.5 mL, 3.61 mmol). The reaction mixture was stirred at 95°C for 2 h and then at room temperature for 17 h. The reaction was diluted with water and ethyl acetate. The organic phase was washed with water and brine, dried over $MgSO_4$, then filtered. The filtrate was adsorbed onto isolute and purified by silica gel chromatography to give the title compound (98 mg, 15%). LC-MS $[M+H]^+$ 360, rt 0.81 min. 1H NMR (400 MHz, methanol-d_4) δ 7.89 (s, 1H), 7.66 (d, J=8.5 Hz, 1H), 7.44 - 7.51 (m, 2H), 7.26 - 7.31 (m, 1H), 7.19 - 7.24 (m, 1H), 4.74 (t, J=8.0 Hz, 1H), 4.64 (s, 2H), 4.29 (s, 3H), 3.56 (s, 3H), 3.21 (dd, J=7.9, 3.9 Hz, 2H).

(*S*)-Methyl 3-(4-chloro-3-((N-methylphenylsulfonamido)methyl)phenyl)-3-(1-methyl-1H-benzo[d][1,2,3]triazol-5-yl)propanoate (21)

A stirred solution of methyl 3-(4-chloro-3-(hydroxymethyl)phenyl)-3-(1-methyl-1H-benzo[d][1,2,3]triazol-5-yl)propanoate (0.485 g, 1.348 mmol), N-methylbenzenesulfonamide (0.243 g, 1.419 mmol), and (*E*)-diazene-1,2-diylbis(piperidin-1-ylmethanone) (0.715 g, 2.83 mmol) in tetrahydrofuran (THF) (18 mL) at 0 °C was treated with tributylphosphine (0.75 mL, 3.04 mmol). Upon addition the colour turned from deep orange to a lighter yellow. The ice-bath was removed and the solution allowed stirred at ambient temperature for 15 h during which time a precipitate formed. The supernatant was removed and the solution diluted with acetone and ethyl acetate and washed with water (2x), brine (1x), dried over $MgSO_4$, filtered and concentrated to give a yellow oil. This was adsorbed onto isolute and purified by silica gel chromatography to give a white solid, which was subjected to chiral SFC HPLC resolution to give (*R*)-methyl 3-(4-chloro-3-((N-methylphenylsulfonamido)methyl)phenyl)-3-(1-methyl-1H-

1,2,3-benzotriazol-5-yl)propanoate (0.106 g, 15%) and (S)-methyl 3-(4-chloro-3-((N-methylphenylsulfonamido) methyl)phenyl)-3-(1-methyl-1H-benzo[d][1,2,3]triazol-5-yl)propanoate (0.113 g, 16%). LC-MS $[M+H]^+$ 513/515 (Cl), rt 1.08 min. ^{1}H NMR (400 MHz, methanol-d_4) δ 7.83 - 7.90 (m, 3H), 7.59 - 7.72 (m, 4H), 7.45 (d, J=8.8 Hz, 1H), 7.41 (s, 1H), 7.29 - 7.34 (m, 1H), 7.21 - 7.27 (m, 1H), 4.72 (t, J=7.9 Hz, 1H), 4.27 - 4.34 (m, 5H), 3.58 (s, 3H), 3.14 - 3.22 (m, 2H), 2.62 (s, 3H).

2-Methoxy-6-nitroaniline (23)

A stirred solution of 2-amino-3-nitrophenol (35 g, 227 mmol) in DMF (400 mL) was treated with K_2CO_3 (37.7 g, 273 mmol) and iodomethane (17.04 mL, 273 mmol). After 16 h the mixture was poured into water. The resulting precipitate was collected by filtration and the solid was washed with water and dried to give the title compound (35 g, 89%). LC-MS $[M+H]^+$ 169, rt 1.71 min. ^{1}H NMR (400 MHz, DMSO-d_6) δ 7.59 (m, 1H), 7.08 (m, 3H), 6.62 (m, 1H), 3.88 (s, 3H).

4-Bromo-2-methoxy-6-nitroaniline (24)

A solution of 2-methoxy-6-nitroaniline (35 g, 208 mmol) in acetic acid (500 mL) was treated with sodium acetate (27.3 g, 333 mmol) and bromine (11.80 mL, 229 mmol). Then the reaction mixture was stirred at room temperature for 20 minutes. The resulting precipitate was filtered and washed with water and dried in-vacuum pump to give 50 g (95%) of the title compound. LC-MS $[M+H]^+$ 249, rt 1.78 min. ^{1}H NMR (400 MHz, DMSO-d_6) δ 7.75 (s, 1 H), 7.22 (m, 3 H), 3.92 (s, 3 H).

4-Bromo-2-methoxy-N-methyl-6-nitroaniline (25)

A stirred solution of 4-bromo-2-methoxy-6-nitroaniline (50 g, 202 mmol) in DMF (400 mL) at 0°C was treated with NaH (5.83 g, 243 mmol). After 30 minutes, iodomethane (13.92 mL, 223 mmol) was added and the reaction mixture was stirred for a further 30 minutes. Water (1000 mL) was added. The red precipitate was collected by filtration, washed with water and dried to give the title compound (50 g, 72%). LC-MS $[M+H]^+$ 263, rt 1.86 min.

4-Bromo-6-methoxy-N1-methylbenzene-1,2-diamine (26)

A stirred solution of 4-bromo-2-methoxy-N-methyl-6-nitroaniline (25 g, 96 mmol) in acetic acid (300 mL), was treated with zinc (18.78 g, 287 mmol) in small portions. Then the reaction mixture was stirred at ambient temperature for 10 h. The reaction mixture was filtered through celite and the solid was washed copiously with EtOAc. The combined solutions were concentrated to give the title compound (20 g, 27.6%). LC-MS $[M+H]^+$ 233, rt 1.25 min. ^1H NMR (400 MHz, $CDCl_3$) δ 7.58 (s, 1H), 6.45 (s, 1H), 3.93 (br s, 2 H), 3.78 (s, 3 H), 2.62 (s, 3 H).

5-Bromo-7-methoxy-1-methyl-1H-benzo[d][1,2,3]triazole (27)

To 4-bromo-6-methoxy-N1-methylbenzene-1,2-diamine (40 g, 173 mmol) in 100 mL of 10% H_2SO_4 at 0°C, sodium nitrite (16.72 g, 242 mmol) was added in small portions over a 20 minute period. After the reaction mixture was stirred for 30 minutes further, 200 mL of water was

added. The resulting precipitate was collected by filtration, washed with water and dried. The mother liquid was left to stand 16 h and a second batch of precipitate formed, which was collected as before. The combined solids were columned in EtOAc to remove inorganic salts, to give the title compound (15 g, 36%). LC-MS $[M+H]^+$ 244, rt 1.68 min. ^{1}H NMR (400 MHz, $CDCl_3$) δ 7.75 (s, 1 H), 6.85 (s, 1 H), 4.48 (s, 3 H), 4.00 (s, 3 H).

(*E*)-Ethyl 3-(7-methoxy-1-methyl-1H-benzo[d][1,2,3]triazol-5-yl)acrylate (28)

To a stirred solution of 5-bromo-7-methoxy-1-methyl-1H-benzo[d][1,2,3]triazole (10 g, 41.3 mmol) in dry DMF (10 mL), ethyl acrylate (20.68 g, 207 mmol), DIPEA (18.04 mL, 103 mmol), and tri-o-tolylphosphine (2.51 g, 8.26 mmol) were added, followed by $Pd(OAc)_2$ (0.927 g, 4.13 mmol). The reaction was heated to 95°C under a nitrogen atmosphere for 4 h. The reaction mixture was diluted with water and extracted with EtOAc (x3). Combined organic fractions were dried over $MgSO_4$ and concentrated. The residue was purified by silica gel chromatography (10-50% EtOAc/Petrol) to give the title compound (9.2 g, 83%). LC-MS $[M+H]^+$ 262, rt 1.70 min. ^{1}H NMR (400 MHz, $CDCl_3$) δ 7.73 - 7.85 (m, 2H), 6.95 (s, 1H), 6.47 (d, J=16.1 Hz, 1H), 4.48 (s, 3H), 4.32 (q, J=7.0 Hz, 2H), 4.05 (s, 3H), 1.38 (t, J=7.2 Hz, 3H).

Ethyl 3-(3-(hydroxymethyl)-4-methylphenyl)-3-(7-methoxy-1-methyl-1H-benzo[d][1,2,3]triazol-5-yl)propanoate (29)

To a solution of (*E*)-ethyl 3-(7-methoxy-1-methyl-1H-benzo[d][1,2,3]triazol-5-yl)acrylate (0.390 g, 1.493 mmol) in 1,4-dioxane (10 mL) and water (5 ml) was added (3-(hydroxymethyl)-4-

methylphenyl)boronic acid (0.372 g, 2.239 mmol), triethylamine (0.312 mL, 2.239 mmol) and $[RhCl(cod)]_2$ (0.041 g, 0.075 mmol). The resulting reaction mixture was stirred at 95 °C for 1 h. The reaction mixture was extracted with EtOAc (3 x 10 mL). The combined organic layer was dried over $MgSO_4$, filtered, concentrated under reduced pressure, and purified by silica gel chromatography to afford the title compound (0.355 g, 62%). LC-MS $[M+H]^+$ 384, rt 0.88 min. ^1H NMR (400 MHz, $CDCl_3$) δ 7.51 (br. s, 1H), 7.26 - 7.29 (m, 1H), 7.12 (s, 2H), 6.62 (s, 1H), 4.62 - 4.71 (m, 3H), 4.42 (s, 3H), 4.07 (q, J=7.1 Hz, 2H), 3.92 (s, 3H), 3.02 - 3.21 (m, 2H), 2.32 (s, 3H), 1.17 (t, J=7.2 Hz, 3H).

(*R*)-2-Fluoro-N-(2-hydroxypropyl)benzenesulfonamide (31)

A solution of (*R*)-1-amino-2-propanol (0.386 mL, 5.00 mmol) in THF (10 mL) and water (2.5 mL) was treated with K_2CO_3 (0.691 g, 5.00 mmol) and then 2-fluorobenzene-1-sulfonyl chloride (0.662 mL, 5 mmol) slowly. The resulting reaction mixture was stirred at room temperature for 66 h. The reaction mixture was diluted with H_2O (10 mL), extracted with EtOAc (20 mL + 2 x 10 mL). The combined organic layers were washed with brine (15 mL), dried over $MgSO_4$, filtered, and concentrated under reduced pressure, to afford the desired product (*R*)-2-fluoro-N-(2-hydroxypropyl)benzenesulfonamide (1.22 g, 104%). LC-MS $[M+H]^+$ 234, rt 0.65 min. ^1H NMR (400 MHz, DMSO-d_6) δ 7.82 (m, 2 H), 7.70 (m, 1 H), 7.40 (m, 2 H), 4.65 (m, 1 H), 3.60 (m, 1 H), 2.78 (m, 2 H), 1.00 (m, 3 H).

(*R*)-4-Methyl-3,4-dihydro-2H-benzo[b][1,4,5]oxathiazepine 1,1-dioxide (32)

A solution of (*R*)-2-fluoro-N-(2-hydroxypropyl)benzenesulfonamide (1.17 g, 5.0 mmol) in DMSO (20 mL) was treated with potassium tert-butoxide (1.68 g, 15.0 mmol). The resulting reaction mixture was heated with at 100 °C for 20 min. The reaction mixture was diluted with H_2O (30 mL), acidified with HCl (1 N) to pH ~6, extracted with EtOAc (3 x 50 mL). The combined organic layer was washed with brine (50 mL), dried over $MgSO_4$, filtered, concentrated under reduced pressure, purified by silica gel chromatography to afford the desired product (*R*)-4-methyl-3,4-dihydro-2H-benzo[b][1,4,5]oxathiazepine 1,1-dioxide (0.842 g, 79%). LC-MS $[M+H]^+$ 214, rt 0.73 min. ^{1}H NMR (400 MHz, $CDCl_3$) δ 7.81 (m, 1H), 7.48 (m, 1H), 7.18 (m, 2H), 4.95 (m, 1H), 4.18 (m, 1H), 3.63 (m, 1H), 3.40 (m, 1H), 1.40 (m, 3H).

Expression and purification of mouse KEAP1 Kelch domain for crystallography

cDNA encoding the Kelch domain of mouse KEAP1 (Uniprot Q9Z2X8, residues 322-624) was cloned into a pET15b vector to incorporate a thrombin-cleavable N-terminal hexahistidine tag. The protein was expressed in BL21 (DE3) cells, using 0.5 mM IPTG for overnight induction at 18^{o}C. Initial purification was carried out using Ni-affinity chromatography followed by removal of the hexahistidine tag by addition of bovine thombin (Sigma). The cleaved protein was incubated with Ni resin and benzamidine sepharose before size-exclusion chromatography using a HiPrep S75 26/60 column (GE Healthcare) equilibrated in 20 mM Tris-HCl pH 8.3, 20 mM DTT and 10 mM benzamidine. The protein was concentrated to 14 mg/mL for crystallography.

Expression and purification of human KEAP1 Kelch domain for FP assay and ITC

cDNA encoding the Kelch domain of human KEAP1 (Uniprot Q14145, residues 321-609) was subcloned into the pDEST8 vector to generate an ORF encoding the Kelch domain with an N-terminal hexahistidine tag, a TEV protease cleavage site, and an Avi tag. Virus was generated using the Bac-to-Bac Baculovirus Expression System (Life Technologies) as per the manufacturer's directions. Protein was expressed in *Spodoptera frugiperda* (Sf9) cells by infection of 2 x 10^6 cells/mL in ExCell 420 medium (SAFC, St. Louis) using the TIPS method.[46] Cells were collected by centrifugation 72 h post-infection and processed for purification of recombinant protein. Harvested cells were resuspended in lysis buffer (50 mM Tris-HCl pH 7.5, 150 mM NaCl, 0.5 mM tris(2-carboxyethyl)phosphine (TCEP)), and disrupted using an EmulsiFlex-C50 homogenizer (Avestin, Ottawa, Ontario, Canada) before clarification by centrifugation. The crude protein was then purified by Ni-affinity chromatography by imidazole gradient elution (0-300 mM imidazole in lysis buffer). The hexahistidine tag was removed by TEV protease cleavage (1:50 TEV to protein ratio (w/w)) during overnight dialysis against 50 mM Tris-HCl, pH 8.0, 150 mM NaCl at 4°C. The protein was subsequently purified by size exclusion chromatography using a 320 mL Superdex 75 column (GE Healthcare) equilibrated in 50 mM Tris-HCl pH 7.5, 150 mM NaCl, 0.5 mM TCEP, and 5% glycerol before concentration to 2.36 mg/mL and storage at −80°C.

Crystallization, ligand soaking and X-ray data collection

Crystallization was by vapour-diffusion using the hanging drop method from 0.3 – 0.6 $(NH_4)_2SO_4$, 0.4 – 1.4 M Li_2SO_4 and 0.1 M Na_3citrate-HCl pH 5.6. To generate protein-ligand complexes, crystals were typically soaked overnight in a solution containing 5 - 50 mM ligand

(formulated from DMSO stocks), 100 mM Bis-Tris pH 7.0, 25% PEG 4K before plunge-freezing in liquid nitrogen. X-ray diffraction data were collected using a Rigaku-MSC Saturn 944+ CCD mounted on an FR-E+ rotating anode generator and processed using Astex's protein-ligand structure pipeline[47] with the apo mouse Kelch structure 1x2j as the starting model. Manual cycles of model adjustment and refinement were carried out using AstexViewer,[48] Coot[49] and Refmac.[50] Data collection and refinement statistics are presented in supplemental Table S2.

KEAP1 Kelch fluorescence polarisation (FP) assay

Inhibition of the Kelch domain-NRF2 interaction was determined using a fluorescence polarisation-based competition assay in a black 384-well microplate (Corning 3573). Each well contained 2 nM 5'-TAMRA-NRF2 peptide (AFFAQLQLDEETGEFL) and 7 nM human KEAP1 (residues 321-609) in 50 µL of assay buffer (50 mM Tris-HCl pH 8.0, 100 mM NaCl, 5 mM $MgCl_2$, 2 mM 3-[(3-Cholamidopropyl)dimethylammonio]-1-propanesulfonate (CHAPS), 1 mM DTT, 0.005% BSA, 1% DMSO). After 1 hour at room temperature, fluorescence polarisation (excitation 485 nm/emission 520 nm) was measured using a BMG Pherastar FS plate reader. IC_{50} values were determined by fitting the data to a four parameter logistic fit using Graphpad Prism 6.0.

Isothermal Titration Calorimetry

ITC experiments were performed on a Microcal VP-ITC (Malvern Instruments Ltd) at 25°C in a buffer comprising 50 mM 4-(2-hydroxyethyl)-1-piperazineethanesulfonic acid (HEPES)-NaOH pH 7.5, 100 mM NaCl, 1 mM TCEP and 5% DMSO. For all experiments compound was in the

syringe and protein (human KEAP1 residues 321-609) was in the sample cell. Data analysis was performed using Origin 7.0 software. Heats of dilution were estimated using the final injections of each individual titration and subtracted before data analysis.

Cell-based and in vivo studies

The human lung has an intricate composition of various cell types. For our purposes, the human lung cells used for the *in vitro* experiments included the BEAS-2B cell line (American Type Culture Collection, ATCC), Normal Human Bronchial Epithelial Cells (Lonza, Walkersville, MD) obtained from healthy individual donors, and epithelial cells (bronchial brushings) from COPD subjects (provided by Dr. Steven Kelsen at The Center for Inflammation, Translational and Clinical Lung Research Laboratory at Temple University, protocol number 11764 approved by the IRB at Temple University).

NRF2 translocation in NHBE cells

NHBE cells (Lonza, Walkersville, MD) were plated in 100 mm culture dishes at 3 x 10^6 cells per plate and cultured for 48 hours or until >80% confluent in BEGM medium (Lonza, Walkersville, MD). On the day of the study cells were treated with DMSO (0.1% final) or compounds for 6 hours at 37°C, 5% CO_2. Cellular fractions were made using a modified version of the protocol for the NRF2 Trans Am kit (Active Motif, Carlsbad, CA). Briefly, cells were washed with ice cold PBS and then removed from the plate using a cell scraper in 5 mL ice cold PBS with protease inhibitor buffer. The cells were then centrifuged and resuspended in hypotonic buffer

and allowed to swell on ice for 15 minutes. Twenty-five microliters of 10% Nonidet P-40 was added and the cells were vortexed. The supernatant (cytoplasmic fraction) was removed after centrifugation at 4°C and the pellet was re-suspended in complete lysis buffer and incubated for 30 minutes, rocking at 4°C. Samples were centrifuged for 10 minutes at 4°C and the supernatant (nuclear fraction) was removed. Protein concentration was determined by the Bradford assay (Bio-Rad, Saint Louis, MO) and NRF2 protein levels were assayed using the Trans Am kit. Data is reported as the OD_{450} per µg total protein as a percent of DMSO control. Data shown is the mean and SEM of 5 independent experiments using GraphPad Prism V5.

Gene Expression in NHBE Cells Transfected with NRF2 siRNA

NHBE cells were plated at passage 5 and were transfected with non-targeting or NRF2 siRNAs (Thermo Scientific/Dharmacon) for 48 hours. The cells were treated with compound **7** on day two post-transfection for approximately 24 hours at 37°C and 5% CO_2. RNA was isolated and quantified using GE Healthcare's Illustra RNA spin Mini Kit. The cDNA was amplified according to Qiagen's QuantiTect® Reverse Transcription Handbook with Qiagen's Reverse Transcriptase Kit. The Human 18s rRNA, *NQO1*, or *GCLM* primer and probe sets and Taqman® Fast Advanced Master Mix were from Applied Biosystems. The 384 well format was used on a ViiA 7 (Applied Biosystems) Real-Time PCR System. The data was analyzed and exported using Applied Biosystem's ViiA 7 software 1.1. Target fold changes were determined by the Livak method.[52] The calculated results were graphed using GraphPad (La Jolla, CA) and show the mean target fold change of three samples (n=1 experiment, representative of three studies).

NQO1 Activity in NHBE Cells Transfected with NRF2 siRNA

NHBE cells (Lonza, passages: 3) were plated in complete BEGM medium (Lonza) and were incubated overnight. The cells were then transfected with 25 nM non-targeting or NRF2 siRNA (Thermo Scientific/Dharmacon, Lafayette CO) for 48 hours. The cells were treated with DMSO (0.1% final) or compounds for an additional 48 hours at 37°C, 5% CO_2. The cells were lysed and the samples were assayed for protein concentration using the Bradford Assay (Bio Rad, Hercules CA). NQO1 activity was then assessed using a modified assay based on Prochaska.[51] The absorbance was monitored using an Envision Multi-label plate reader at 570 nm for 30 minutes. Enzyme activity was determined by the equation: Activity Units (mmol/min) = [ΔOD per min/11300M^{-1}cm (extinction coefficient)] × [volume in μL] × 10^6. In order to determine NQO1 specific activity, samples were assayed in parallel with and without the NQO1 inhibitor dicoumarol, and the values obtained with dicoumarol were subtracted from those without. The samples were then normalized to total protein level and represented as μmol/min/mg total protein. Values were converted to percent of DMSO control and concentration response curves are analyzed in Graphpad Prism v 5.0 by performing a log [agonist] *versus* Response – Variable slope (three parameters) analysis using a bottom constraint of >100%. Data shown is a representative example of two independent experiments.

BEAS-2B NQO1 MTT Assay

BEAS-2B cells (ATCC) were plated in 384 well black clear-bottomed plates and were incubated overnight (37°C, 5% CO_2). On day 2, the plates were centrifuged and 50 nL of compound or controls were added to the cells for 48 hours. On day 4, the medium was aspirated from the plate

and crude cell lysates were made by using 1X (Cell Signaling Technology, Boston MA) lysis buffer with Complete, Mini, EDTA-free Protease Inhibitor (Roche Applied Sciences, Germany). After lysis, the plates were incubated for 20 minutes at RT and the MTT cocktail was prepared for measurement of NQO1 activity.[51] The samples were analyzed on an Envision plate reader (Perkin Elmer), reading absorbance at 570 nm for five individual readings with 10 minute intervals. Product formation was measured kinetically and the pEC_{50} of NQO1 specific activity induction was calculated by plotting the change in absorbance (ΔOD/min) *versus* log [compound] followed by 4-parameter fitting with GraphPad Prism v 5.03 (La Jolla, CA).

Glutathione Assay

Normal Human Bronchial Epithelial Cells (NHBEs, Lonza, Walkersville, MD) were cultured according to the manufacturer and were used at passage 4. NHBE cells were treated the following day with DMSO, CDDO-Me (0.001-0.1 μM) or compound **7** (0.0003-1 μM) for 18 hours. The cells were then treated with tBHP (300 μM), Buthionine Sulfoximine (BSO, 3 mM), or N-Acetylcysteine (NAC, 1 mM) (Sigma) for 4 hours (5% CO_2 and 37°C). The cells were assayed for glutathione content according to the manufacturer's protocol (Arbor Assays DetectX® Glutathione Fluorescent Detection Kit, Ann Arbor, MI). Results are representative of three separate experiments and expressed in μM based on a standard curve.

Air Liquid Interface with COPD lung cells and culture conditions

Human bronchoscopic bronchial brushings were obtained from COPD patients following informed consent. The cells obtained from the bronchial brushes were centrifuged. The pellet was then seeded into one collagen-coated T75 cm^2 flask until cells were 90% confluent before transferring them into T150 cm^2 flask for expansion. The human bronchial epithelial cells were grown in supplemented BEBM (Lonza), supplemented with 100 ng/mL retinoic acid (Sigma) and 25 ng/mL recombinant human epidermal growth factor (Sigma). Cells were cultured at 37ºC in a humidified atmosphere of 5% CO_2 with the culture medium changed three times weekly.

Air liquid interface culture (ALI culture) with COPD lung cells and Gene Expression

Air liquid interface cultures were grown using a 1:1 mixture of BEBM (Lonza) and DMEM. Cells from subjects used in this study were grown at ALI at passage 2. The cells were grown on transwell-24 well permeable membranes (0.4 μM pore size, polyester membrane) and were submerged for the first 3 days, during which time the culture medium was changed on day 1 and every other day thereafter. ALI was created once the cells reached 100% confluence. The apical medium was removed and the culture medium on the basolateral side was changed every other day until the cells were differentiated at approximately 28 days.

RNA extraction and real-time PCR analysis for ALI Gene Expression and in vivo Studies

Total RNA was isolated using GE Healthcare RNAspin Mini RNA isolation kit (GE Heatlhcare, USA) or Trizol reagent (Life Technologies) according to the manufacturer's instructions and quantified using an Agilent RNA 6000 Nano instrument. Real-time PCR was performed on the

ABI prism 7900HT sequence detector (Applied Biosystems) using 18S rRNA as the internal control. The cDNA was amplified with specific primers for HO-1/*Ho-1*, NQO1/*Nqo1*, TXNRD1/*Txnrd1*, SRXN1/*Srxn1*, GCLC/*Gclc*, GCLM/*Gclm*, GSTA3/*Gsta3* using universal master mix (Applied Biosystems). The primers/probes sets used for amplification of cDNA was obtained from TaqMan Gene Expression Assays (Applied Biosystems). An identical threshold cycle (C_T) was applied for each gene of interest. The comparative C_T ($\Delta\Delta C_T$) relative quantification method was used to calculate the relative mRNA levels of target genes as described in the Applied Biosystems Chemistry Guide.

Compound 7 Pharmacokinetics

In order to inform the *in vivo* dosing regimen for compound **7**, pharmacokinetic data were determined in the Han Wistar rat. Compound **7** was dosed in a standard IV/PO crossover design (n=3) separated by a two day washout period. Blood samples were collected over a 24 hour period and analyzed by LC/MS/MS to acquire concentrations. Subsequent analysis of blood concentrations with Phoenix Winnonlin software yielded the pharmacokinetic parameters presented in supplemental Figure S4.

Compound 7 IV Dose Response and mRNA Expression

Compound **7** exposure was determined following a six hour IV infusion at 1.5 mL/hr in male Han Wistar rats (Charles River). Five animals per group received an IV infusion of a vehicle (25 mM Tris Buffered Saline, 7.8) or of compound **7** delivered at 1.5 mL/hr at various concentrations

to achieve a final, targeted total delivered dose of: 5, 10, 25, and 50 μmol/kg. Lungs were collected following infusion and frozen for analysis of mRNA expression.

Rat Ozone Model

Han Wistar rats (250 – 300 g, Charles River) were randomly designated to the following treatment groups (n=8/group): Air + Vehicle, Ozone (O_3) + Vehicle, Ozone (O_3) + compound **7** at the indicated doses. Twenty-four hours prior to ozone injury, rats were administered intravenous (IV) infusion of compound **7** or vehicle for a 6 hour period. O_3 was generated by an Oxycycler ozonator (model A84ZV, Biospherix Inc. Lacona, NY) in which compressed air and oxygen was passed through the ozonator and flowed into a plexiglass chamber containing the rodents. Rats were exposed to 1 ppm of ozone for a 3 h period. Ozone concentrations, humidity and CO_2 within the chamber were constantly monitored by the Oxycycler watview software and using an independent ozone monitor (Model 465L, Teledyne Advanced Pollution Instrumentation, Inc). The rats were euthanized 15 min after injury by IP administration of 1 mL of Fatal Plus (Vortech Pharmaceuticals, Dearborn, MI). For collection of BAL cells, the tracheas were cannulated, and the lungs were aspirated with a 3 mL aliquot of ice cold PBS. After collection, the BAL fluid was centrifuged at 400 *g* for 2 minutes. The resulting cell pellets were resuspended in a 1 mL aliquot of PBS, and total cells were counted using a hemocytometer. Differential cell analysis was performed on cytospins using Wright-Giemsa stain. For analysis of GSH, lungs were snap frozen and stored at -80°C until use. GSH content was determined using a glutathione assay kit (Cayman Chemicals, Ann Arbor, MI) according to the

manufacturer's instructions. Blood samples were collected at several time points during the 6 hour IV infusion, and analyzed for concentrations of compound **7** by LC/MS/MS.

Rodents were housed in pathogen-free conditions in the Lab Animal Science facility at GlaxoSmithKline Pharmaceuticals according to institutional, state and federal guidelines and had free access to food and water. All animal protocols were reviewed and approved by the Animal Use and Care Committees of GlaxoSmithKline Pharmaceuticals.

AUTHOR INFORMATION

Corresponding Authors

*T.D.H. Tel: +44 (0) 1223 226270. Fax: +44 (0) 1223 226201. Email: Tom.Heightman@astx.com

*J.K.K. Tel: +1 610-270-6579. Fax: +1 610-270-4451. Email: Jeffrey.K.Kerns@gsk.com

Author Contributions

Experimental design: TGD, JEC, CGJ, DN, CR, GS, HMGW, AJAW, TDH, WEW, JECot., JPK, JGY, HGF, YS, JPF, PLP, HY, JFC, JKK. *Performed experiments:* TGD, JEC, CGJ, KH, RM, DN, SJR, CR, AJAW, TDH, WEW, JECot., JPK, JGY, JPF, BJB, GL, HY, JKK. *Data analysis:* TGD, JEC, CGJ, KH, RM, DN, SJR, CR, GS, HMGW, AJAW, TDH, WEW, JECot., JPK, JGY, HGF, YS, JPF, BJB, GL, PLP, HY, JKK. *Wrote the manuscript:* TGD, TDH, WEW, JECot., JPK, JGY, HGF, YS, JPF, PLP, HY, JFC, JKK.

ACKNOWLEDGEMENTS

The authors thank Philip Day for the cloning of mouse Kelch, Kirsten Smith and Anne Cleasby for protein expression/purification, Finn Holding for mass spectrometry, Lawrence Wolfe and Michael Fischer for the NQO1 activity screening assay, Thomas Sweitzer for efforts with the eXP data, Wangfang Hou for molecular biology and expression work for the human KEAP1 Kelch domain, Hongwei Qi for purification of human KEAP1 Kelch domain, and Catherine Boothe-Genthe, Casey Kmett, Sandy Umbrecht, Brian Peck, Philip Landis for their efforts with the methods and pharmacokinetic data for compound **7**. We would also like to thank Dr. Steven Kelsen, his colleagues, and donors who provided lung samples to support our studies. The authors would like to thank Robin Carr for his continued support for the project.

ABBREVIATIONS

ALI, air-liquid interface; ARE, antioxidant response element; BAL, bronchoalveolar lavage; BSEP, bile salt export pump; BSO, buthionine sulfoxide; BTB, Broad-complex, Tramtrack and Bric-a-Brac; CDDO, 2-cyano-3,12-dioxooleana-1,9-dien-28-oic-acid; CHAPS, 3-[(3-Cholamidopropyl)dimethylammonio]-1-propanesulfonate; COPD, Chronic obstructive pulmonary disease; DIAD, diisopropyl azodicarboxylate; FP, fluorescence polarization; GSH, glutathione; HEPES, 4-(2-hydroxyethyl)-1-piperazineethanesulfonic acid; ITC, Isothermal Scanning Calorimetry; IVR, Intervening Region; KEAP1, Kelch-like ECH-associated protein 1; NAC, N-acetyl cysteine; NHBE, Normal Human Bronchial Epithelial; NQO1, NAD(P)H:quinone acceptor oxidoreductase 1; NRF2, Nuclear factor erythroid 2–related factor 2; OATP1B1, Organic Anion Transporting Polypeptide 1B1; TCEP, tris(2-carboxyethyl)phosphine; tBHP, tert-Butyl Hydroperoxide; tBHQ, tert-butylhydroquinone.

ASSOCIATED CONTENT

PDB ID Codes

Coordinates and structure factors for the KEAP1-ligand complex have been deposited with PDB with accession codes: 5fnq (KEAP1-**1**), 5fzj (KEAP1-**2**), 5fzn (KEAP1-**3**), 5fnr (KEAP1-**4**), 5fns (KEAP1-**5**), 5fnt (KEAP1-**6**) and 5fnu (KEAP1-**7**).

Supporting Information

The following Figures and Tables are provided as Supporting Information:

Figure S1 Compound **7** increases NRF2 nuclear translocation in NHBE cells

Figure S2 Effect of *NRF2* siRNA transfection on *NRF2* mRNA expression in NHBE cells

Figure S3 Morphological changes in NHBE cells

Figure S4 Pharmacokinetic data for compound **7** in Han Wistar rat

Figure S5 ^{1}H NMR spectrum for compound **7**

Table S1 Enhanced Cross-screen Panel (eXP) results for compound **7**

Table S2 X-ray data collection and refinement statistics

REFERENCES

(1) Itoh, K.; Chiba, T.; Takahashi, S.; Ishii, T.; Igarashi, K.; Katoh, Y.; Oyake, T.; Hayashi, N.; Satoh, K.; Hatayama, I.; Yamamoto, M.; Nabeshima, Y. An Nrf2/small Maf heterodimer mediates the induction of phase II detoxifying enzyme genes through antioxidant response elements. *Biochem. Biophys. Res. Commun.* **1997,** *236*, 313-322.

(2) Wakabayashi, N.; Dinkova-Kostova, A. T.; Holtzclaw, W. D.; Kang, M. I.; Kobayashi, A.; Yamamoto, M.; Kensler, T. W.; Talalay, P. Protection against electrophile and oxidant stress by induction of the phase 2 response: fate of cysteines of the Keap1 sensor modified by inducers. *Proc. Natl. Acad. Sci. U.S.A.* **2004,** *101*, 2040-2045.

(3) Zhang, M.; An, C.; Gao, Y.; Leak, R. K.; Chen, J.; Zhang, F. Emerging roles of Nrf2 and phase II antioxidant enzymes in neuroprotection. *Prog. Neurobiol.* **2013,** *100*, 30-47.

(4) Zhang, D. D.; Lo, S. C.; Cross, J. V.; Templeton, D. J.; Hannink, M. Keap1 is a redox-regulated substrate adaptor protein for a Cul3-dependent ubiquitin ligase complex. *Mol. Cell Biol.* **2004,** *24*, 10941-10953.

(5) Cullinan, S. B.; Gordan, J. D.; Jin, J.; Harper, J. W.; Diehl, J. A. The Keap1-BTB protein is an adaptor that bridges Nrf2 to a Cul3-based E3 ligase: oxidative stress sensing by a Cul3-Keap1 ligase. *Mol. Cell Biol.* **2004,** *24*, 8477-8486.

(6) Canning, P.; Cooper, C. D.; Krojer, T.; Murray, J. W.; Pike, A. C.; Chaikuad, A.; Keates, T.; Thangaratnarajah, C.; Hojzan, V.; Marsden, B. D.; Gileadi, O.; Knapp, S.; von, D. F.;

Bullock, A. N. Structural basis for Cul3 protein assembly with the BTB-Kelch family of E3 ubiquitin ligases. *J. Biol. Chem.* **2013,** *288*, 7803-7814.

(7) Li, X.; Zhang, D.; Hannink, M.; Beamer, L. J. Crystal structure of the Kelch domain of human Keap1. *J. Biol. Chem.* **2004,** *279*, 54750-54758.

(8) Cleasby, A.; Yon, J.; Day, P. J.; Richardson, C.; Tickle, I. J.; Williams, P. A.; Callahan, J. F.; Carr, R.; Concha, N.; Kerns, J. K.; Qi, H.; Sweitzer, T.; Ward, P.; Davies, T. G. Structure of the BTB domain of Keap1 and its interaction with the triterpenoid antagonist CDDO. *PLoS One* **2014,** *9*, e98896.

(9) Zhang, D. D.; Hannink, M. Distinct cysteine residues in Keap1 are required for Keap1-dependent ubiquitination of Nrf2 and for stabilization of Nrf2 by chemopreventive agents and oxidative stress. *Mol. Cell Biol.* **2003,** *23*, 8137-8151.

(10) Dinkova-Kostova, A. T.; Holtzclaw, W. D.; Cole, R. N.; Itoh, K.; Wakabayashi, N.; Katoh, Y.; Yamamoto, M.; Talalay, P. Direct evidence that sulfhydryl groups of Keap1 are the sensors regulating induction of phase 2 enzymes that protect against carcinogens and oxidants. *Proc. Natl. Acad. Sci. U.S.A.* **2002,** *99*, 11908-11913.

(11) Rachakonda, G.; Xiong, Y.; Sekhar, K. R.; Stamer, S. L.; Liebler, D. C.; Freeman, M. L. Covalent modification at Cys151 dissociates the electrophile sensor Keap1 from the ubiquitin ligase CUL3. *Chem. Res. Toxicol.* **2008,** *21*, 705-710.

(12) Eggler, A. L.; Small, E.; Hannink, M.; Mesecar, A. D. Cul3-mediated Nrf2 ubiquitination and antioxidant response element (ARE) activation are dependent on the partial molar volume at position 151 of Keap1. *Biochem. J.* **2009,** *422*, 171-180.

(13) Kensler, T. W.; Wakabayashi, N.; Biswal, S. Cell survival responses to environmental stresses via the Keap1-Nrf2-ARE pathway. *Annu. Rev. Pharmacol. Toxicol.* **2007,** *47*, 89-116.

(14) Wasserman, W. W.; Fahl, W. E. Functional antioxidant responsive elements. *Proc. Natl. Acad. Sci. U.S.A.* **1997,** *94*, 5361-5366.

(15) Cho, H. Y.; Kleeberger, S. R. Nrf2 protects against airway disorders. *Toxicol. Appl. Pharmacol.* **2010,** *244*, 43-56.

(16) Boutten, A.; Goven, D.; Artaud-Macari, E.; Boczkowski, J.; Bonay, M. NRF2 targeting: a promising therapeutic strategy in chronic obstructive pulmonary disease. *Trends Mol. Med.* **2011,** *17*, 363-71.

(17) Calkins, M. J.; Johnson, D. A.; Townsend, J. A.; Vargas, M. R.; Dowell, J. A.; Williamson, T. P.; Kraft, A. D.; Lee, J. M.; Li, J.; Johnson, J. A. The Nrf2/ARE pathway as a potential therapeutic target in neurodegenerative disease. *Antioxid. Redox. Signal.* **2009,** *11*, 497-508.

(18) Li, J.; Ichikawa, T.; Janicki, J. S.; Cui, T. Targeting the Nrf2 pathway against cardiovascular disease. *Expert. Opin. Ther. Targets* **2009,** *13*, 785-794.

(19) Pergola, P. E.; Raskin, P.; Toto, R. D.; Meyer, C. J.; Huff, J. W.; Grossman, E. B.; Krauth, M.; Ruiz, S.; Audhya, P.; Christ-Schmidt, H.; Wittes, J.; Warnock, D. G. Bardoxolone methyl and kidney function in CKD with type 2 diabetes. *N. Engl. J. Med.* **2011,** *365*, 327-336.

(20) Wilson, A. J.; Kerns, J. K.; Callahan, J. F.; Moody, C. J. Keap calm - and carry on covalently. *J. Med. Chem.* **2013,** *56*, 7463-7476.

(21) Sussan, T. E.; Rangasamy, T.; Blake, D. J.; Malhotra, D.; El-Haddad, H.; Bedja, D.; Yates, M. S.; Kombairaju, P.; Yamamoto, M.; Liby, K. T.; Sporn, M. B.; Gabrielson, K. L.; Champion, H. C.; Tuder, R. M.; Kensler, T. W.; Biswal, S. Targeting Nrf2 with the triterpenoid CDDO-imidazolide attenuates cigarette smoke-induced emphysema and cardiac dysfunction in mice. *Proc. Natl. Acad. Sci. U.S.A.* **2009,** *106*, 250-255.

(22) Hu, C.; Eggler, A. L.; Mesecar, A. D.; van Breemen, R. B. Modification of keap1 cysteine residues by sulforaphane. *Chem. Res. Toxicol.* **2011,** *24*, 515-521.

(23) Linker, R. A.; Lee, D. H.; Ryan, S.; van Dam, A. M.; Conrad, R.; Bista, P.; Zeng, W.; Hronowsky, X.; Buko, A.; Chollate, S.; Ellrichmann, G.; Bruck, W.; Dawson, K.; Goelz, S.; Wiese, S.; Scannevin, R. H.; Lukashev, M.; Gold, R. Fumaric acid esters exert neuroprotective effects in neuroinflammation via activation of the Nrf2 antioxidant pathway. *Brain* **2011,** *134*, 678-692.

(24) Padmanabhan, B.; Tong, K. I.; Ohta, T.; Nakamura, Y.; Scharlock, M.; Ohtsuji, M.; Kang, M. I.; Kobayashi, A.; Yokoyama, S.; Yamamoto, M. Structural basis for defects of Keap1 activity provoked by its point mutations in lung cancer. *Mol. Cell* **2006,** *21*, 689-700.

(25) Lo, S. C.; Li, X.; Henzl, M. T.; Beamer, L. J.; Hannink, M. Structure of the Keap1:Nrf2 interface provides mechanistic insight into Nrf2 signaling. *EMBO J.* **2006,** *25*, 3605-3617.

(26) Tong, K. I.; Katoh, Y.; Kusunoki, H.; Itoh, K.; Tanaka, T.; Yamamoto, M. Keap1 recruits Neh2 through binding to ETGE and DLG motifs: characterization of the two-site molecular recognition model. *Mol. Cell Biol.* **2006,** *26*, 2887-2900.

(27) Tong, K. I.; Padmanabhan, B.; Kobayashi, A.; Shang, C.; Hirotsu, Y.; Yokoyama, S.; Yamamoto, M. Different electrostatic potentials define ETGE and DLG motifs as hinge and latch in oxidative stress response. *Mol. Cell Biol.* **2007,** *27*, 7511-7521.

(28) Padmanabhan, B.; Tong, K. I.; Kobayashi, A.; Yamamoto, M.; Yokoyama, S. Structural insights into the similar modes of Nrf2 transcription factor recognition by the cytoplasmic repressor Keap1. *J. Synchrotron. Radiat.* **2008,** *15*, 273-276.

(29) Steel, R.; Cowan, J.; Payerne, E.; O'Connell, M. A.; Searcey, M. Anti-inflammatory Effect of a Cell-Penetrating Peptide Targeting the Nrf2/Keap1 Interaction. *ACS Med. Chem. Lett.* **2012,** *3*, 407-410.

(30) Hu, L.; Magesh, S.; Chen, L.; Wang, L.; Lewis, T. A.; Chen, Y.; Khodier, C.; Inoyama, D.; Beamer, L. J.; Emge, T. J.; Shen, J.; Kerrigan, J. E.; Kong, A. N.; Dandapani, S.; Palmer, M.; Schreiber, S. L.; Munoz, B. Discovery of a small-molecule inhibitor and cellular probe of Keap1-Nrf2 protein-protein interaction. *Bioorg. Med. Chem. Lett.* **2013,** *23*, 3039-3043.

(31) Jnoff, E.; Albrecht, C.; Barker, J. J.; Barker, O.; Beaumont, E.; Bromidge, S.; Brookfield, F.; Brooks, M.; Bubert, C.; Ceska, T.; Corden, V.; Dawson, G.; Duclos, S.; Fryatt, T.; Genicot, C.; Jigorel, E.; Kwong, J.; Maghames, R.; Mushi, I.; Pike, R.; Sands, Z. A.; Smith, M. A.; Stimson, C. C.; Courade, J. P. Binding mode and structure-activity relationships around direct inhibitors of the Nrf2-Keap1 complex. *ChemMedChem* **2014,** *9*, 699-705.

(32) Marcotte, D.; Zeng, W.; Hus, J. C.; McKenzie, A.; Hession, C.; Jin, P.; Bergeron, C.; Lugovskoy, A.; Enyedy, I.; Cuervo, H.; Wang, D.; Atmanene, C.; Roecklin, D.; Vecchi, M.; Vivat, V.; Kraemer, J.; Winkler, D.; Hong, V.; Chao, J.; Lukashev, M.; Silvian, L. Small molecules inhibit the interaction of Nrf2 and the Keap1 Kelch domain through a non-covalent mechanism. *Bioorg. Med. Chem.* **2013,** *21*, 4011-4019.

(33) Jiang, Z. Y.; Lu, M. C.; Xu, L. L.; Yang, T. T.; Xi, M. Y.; Xu, X. L.; Guo, X. K.; Zhang, X. J.; You, Q. D.; Sun, H. P. Discovery of potent Keap1-Nrf2 protein-protein interaction inhibitor based on molecular binding determinants analysis. *J. Med. Chem.* **2014,** *57*, 2736-2745.

(34) Zhuang, C.; Narayanapillai, S.; Zhang, W.; Sham, Y. Y.; Xing, C. Rapid identification of Keap1-Nrf2 small-molecule inhibitors through structure-based virtual screening and hit-based substructure search. *J. Med. Chem.* **2014,** *57*, 1121-1126.

(35) Shimozono, R.; Asaoka, Y.; Yoshizawa, Y.; Aoki, T.; Noda, H.; Yamada, M.; Kaino, M.; Mochizuki, H. Nrf2 activators attenuate the progression of nonalcoholic steatohepatitis-related fibrosis in a dietary rat model. *Mol. Pharmacol.* **2013,** *84*, 62-70.

(36) Jiang, Z. Y.; Xu, L. L.; Lu, M. C.; Chen, Z. Y.; Yuan, Z. W.; Xu, X. L.; Guo, X. K.; Zhang, X. J.; Sun, H. P.; You, Q. D. Structure-Activity and Structure-Property Relationship and Exploratory in Vivo Evaluation of the Nanomolar Keap1-Nrf2 Protein-Protein Interaction Inhibitor. *J. Med. Chem.* **2015,** *58*, 6410-6421.

(37) Winkel, A. F.; Engel, C. K.; Margerie, D.; Kannt, A.; Szillat, H.; Glombik, H.; Kallus, C.; Ruf, S.; S, G. U.; Riedel, J.; Herling, A. W.; von Knethen, A.; Weigert, A.; Br Uumlne, B.; Schmoll, D. Characterization of RA839, a non-covalent small-molecule binder to Keap1 and selective activator of Nrf2 signalling. *J. Biol. Chem.* **2015,** *290*, 28446-28455.

(38) Davies, T. G.; Tickle, I. J. Fragment screening using X-ray crystallography. *Top. Curr. Chem.* **2012,** *317*, 33-59.

(39) Baker, M. Fragment-based lead discovery grows up. *Nat. Rev. Drug Discov.* **2013,** *12*, 5-7.

(40) Chessari, G.; Buck, I. M.; Day, J. E.; Day, P. J.; Iqbal, A.; Johnson, C. N.; Lewis, E. J.; Martins, V.; Miller, D.; Reader, M.; Rees, D. C.; Rich, S. J.; Tamanini, E.; Vitorino, M.; Ward, G. A.; Williams, P. A.; Williams, G.; Wilsher, N. E.; Woolford, A. J. Fragment-Based Drug

Discovery Targeting Inhibitor of Apoptosis Proteins: Discovery of a Non-Alanine Lead Series with Dual Activity Against cIAP1 and XIAP. *J. Med. Chem.* **2015,** *58*, 6574-88.

(41) Kargl, J.; Brown, A. J.; Andersen, L.; Dorn, G.; Schicho, R.; Waldhoer, M.; Heinemann, A. A selective antagonist reveals a potential role of G protein-coupled receptor 55 in platelet and endothelial cell function. *J. Pharmacol. Exp. Ther.* **2013,** *346*, 54-66.

(42) Rangasamy, T.; Cho, C. Y.; Thimmulappa, R. K.; Zhen, L.; Srisuma, S. S.; Kensler, T. W.; Yamamoto, M.; Petrache, I.; Tuder, R. M.; Biswal, S. Genetic ablation of Nrf2 enhances susceptibility to cigarette smoke-induced emphysema in mice. *J. Clin. Invest.* **2004,** *114*, 1248-1259.

(43) Iizuka, T.; Ishii, Y.; Itoh, K.; Kiwamoto, T.; Kimura, T.; Matsuno, Y.; Morishima, Y.; Hegab, A. E.; Homma, S.; Nomura, A.; Sakamoto, T.; Shimura, M.; Yoshida, A.; Yamamoto, M.; Sekizawa, K. Nrf2-deficient mice are highly susceptible to cigarette smoke-induced emphysema. *Genes Cells* **2005,** *10*, 1113-1125.

(44) Nishida, K.; Ohta, Y.; Ishiguro, I. Modulating role of endogenous reduced glutathione in tert-butyl hydroperoxide-induced cell injury in isolated rat hepatocytes. *Free Radic. Biol. Med.* **1997,** *23*, 453-462.

(45) Yore, M. M.; Kettenbach, A. N.; Sporn, M. B.; Gerber, S. A.; Liby, K. T. Proteomic analysis shows synthetic oleanane triterpenoid binds to mTOR. *PLoS One* **2011,** *6*, e22862.

(46) Wasilko, D. J.; Lee, S. E.; Stutzman-Engwall, K. J.; Reitz, B. A.; Emmons, T. L.; Mathis, K. J.; Bienkowski, M. J.; Tomasselli, A. G.; Fischer, H. D. The titerless infected-cells preservation and scale-up (TIPS) method for large-scale production of NO-sensitive human soluble guanylate cyclase (sGC) from insect cells infected with recombinant baculovirus. *Protein Expr. Purif.* **2009,** *65*, 122-132.

(47) Mooij, W. T.; Hartshorn, M. J.; Tickle, I. J.; Sharff, A. J.; Verdonk, M. L.; Jhoti, H. Automated Protein-Ligand Crystallography for Structure-Based Drug Design. *ChemMedChem* **2006,** *1*, 827-838.

(48) Hartshorn, M. J. AstexViewer: a visualisation aid for structure-based drug design. *J. Comput. Aided Mol. Des.* **2002,** *16*, 871-881.

(49) Emsley, P.; Cowtan, K. Coot: model-building tools for molecular graphics. *Acta Crystallogr. D Biol. Crystallogr.* **2004,** *60*, 2126-2132.

(50) Murshudov, G. N.; Vagin, A. A.; Dodson, E. J. Refinement of Macromolecular Structures by the Maximum-Likelihood Method. *Acta Crystallogr. D* **2004,** *D53*, 240-255.

(51) Prochaska, H. J.; Santamaria, A. B. Direct measurement of NAD(P)H:quinone reductase from cells cultured in microtiter wells: a screening assay for anticarcinogenic enzyme inducers. *Anal. Biochem.* **1988,** *169*, 328-336.

(52) Livak, K. J.; Schmittgen, T. D. Analysis of relative gene expression data using real-time quantitative PCR and the 2(-Delta Delta C(T)) Method. *Methods* **2001,** *25*, 402-408.

Table 1 Elaboration of Fragment **1** to lead compound **7**

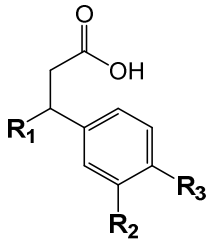

Compound	R_1	R_2	R_3	FP IC_{50} (μM)[a]	ITC K_d (μM)[b]
Fragment 1	H	H	Cl	>1000 (*n*=2)	ND
4	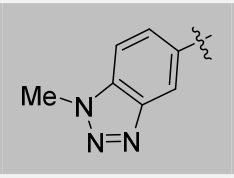	H	Cl	61 (*n*=4)	59[c]
5	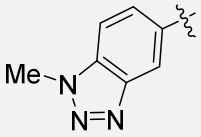	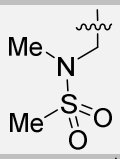	Cl	3.4 (*n*=3)	4.0[c]
6	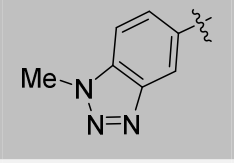	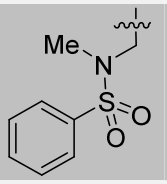	Cl	0.27 (*n*=3)	0.67[c]
7	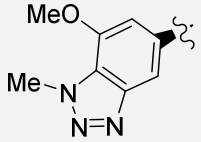	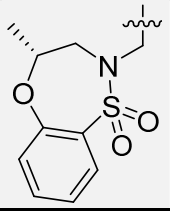	Me	95% I @ 15 nM (*n*=3)	0.0013[d]

[a]Geometric mean of independent determinations. [b]Single determinations. [c]ITC titrations for the racemic compounds **4**, **5**, and **6** yielded standard sigmoidal isotherms indicative of one-site binding, and 1:1 stoichiometries. Any difference in affinity between enantiomers was therefore not sufficiently large to be resolvable from these experiments. [d]The *c*-value ($c = K_d/[KEAP1]$) for the compound **7** data is very high due to tight binding, and so the K_d value quoted here is approximate.

Figure 1

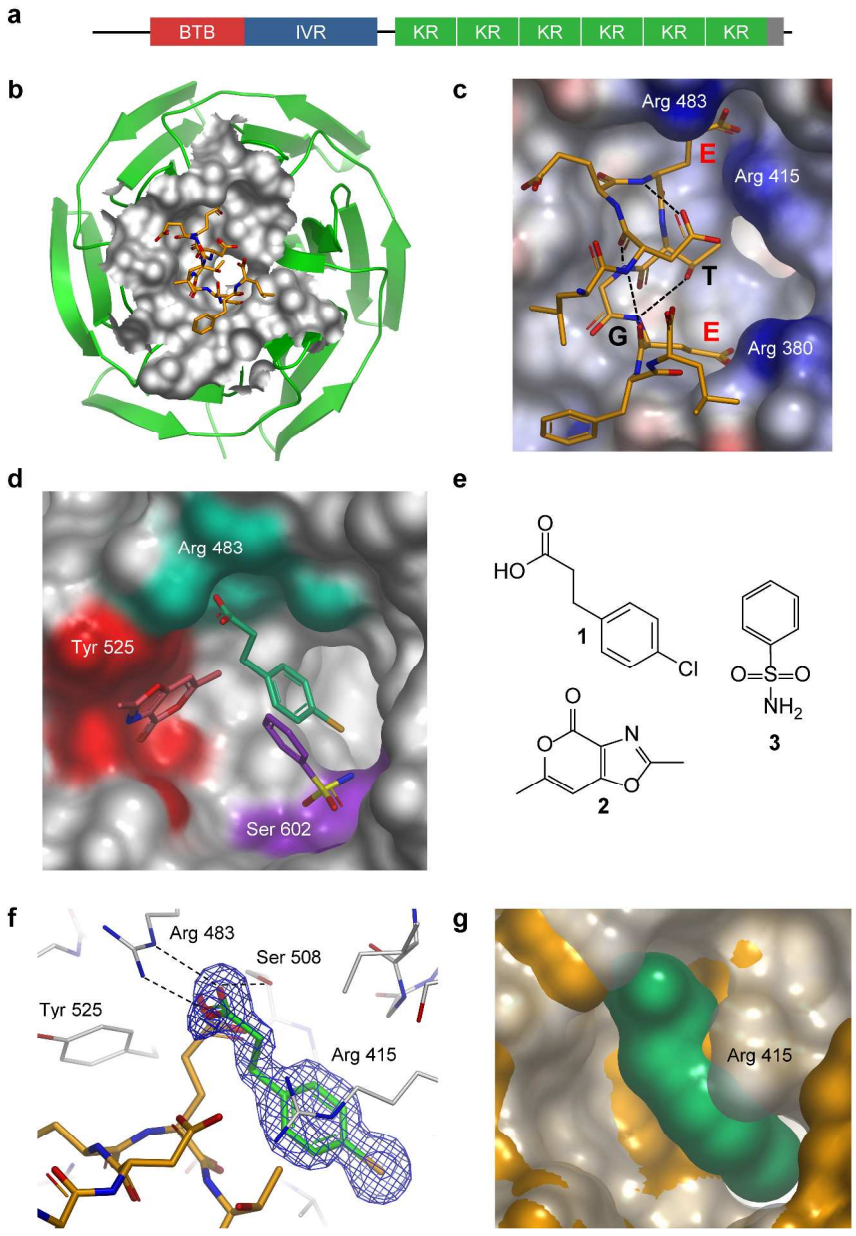
a
BTB
IVR
KR
KR
KR
KR
KR
KR
b
c
Arg 483
E
Arg 415
T
G
E
Arg 380
d
Arg 483
Tyr 525
Ser 602
e
HO
O
1
Cl
O=S=O
NH2
3
O
N
O
O
2
f
Arg 483
Ser 508
Tyr 525
Arg 415
g
Arg 415

Figure 2

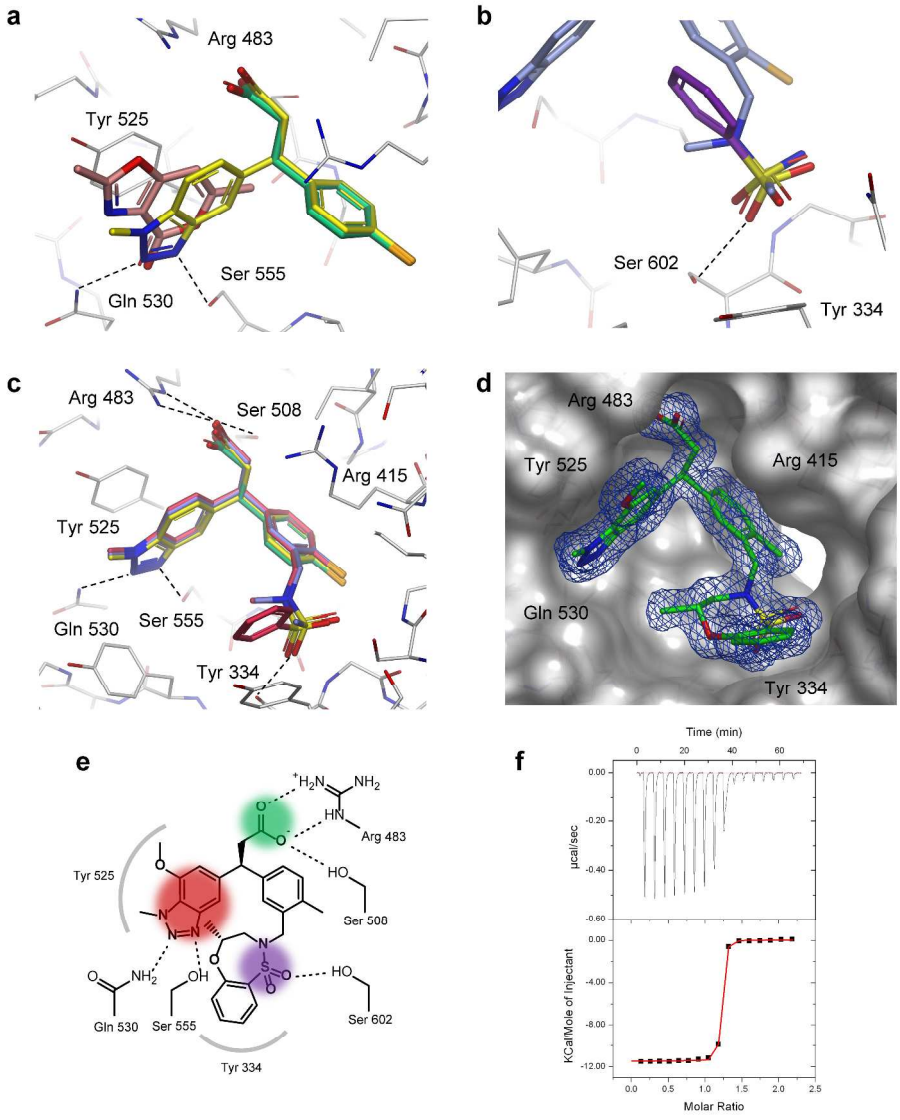
a
Arg 483
Tyr 525
Ser 555
Gln 530
b
Ser 602
Tyr 334
c
Arg 483
Ser 508
Arg 415
Tyr 525
Gln 530
Ser 555
Tyr 334
d
Arg 483
Tyr 525
Arg 415
Gln 530
Tyr 334
e
Arg 483
Tyr 525
Ser 500
Gln 530
Ser 555
Ser 602
Tyr 334
f
Time (min)
µcal/sec
KCal/Mole of injectant
Molar Ratio

Figure 3

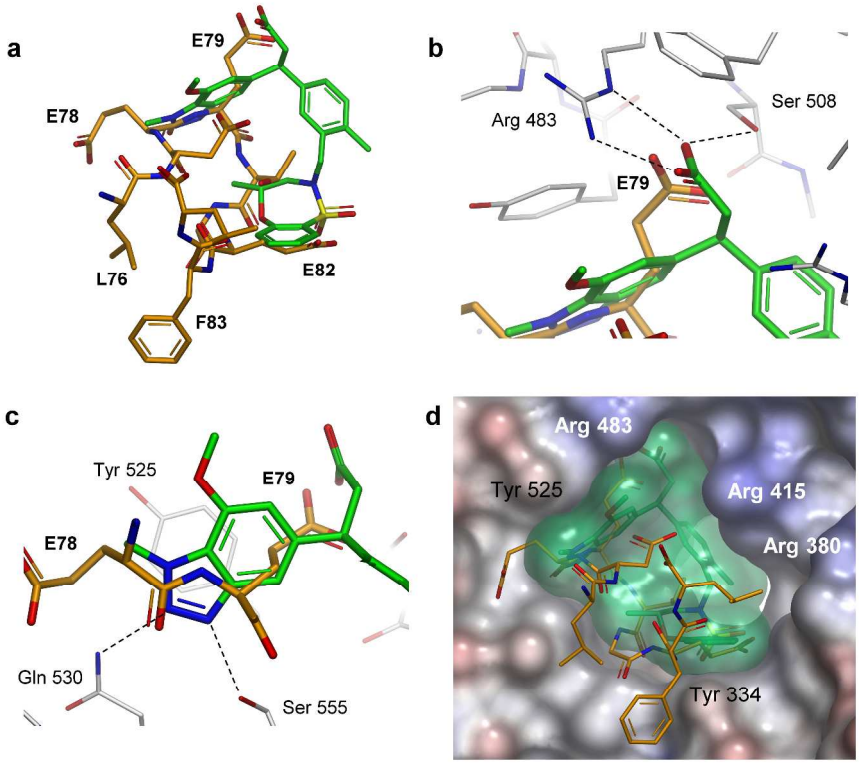
a
E79
E78
L76
E82
F83
b
Arg 483
Ser 508
E79
c
Tyr 525
E79
E78
Gln 530
Ser 555
d
Arg 483
Tyr 525
Arg 415
Arg 380
Tyr 334

Figure 4

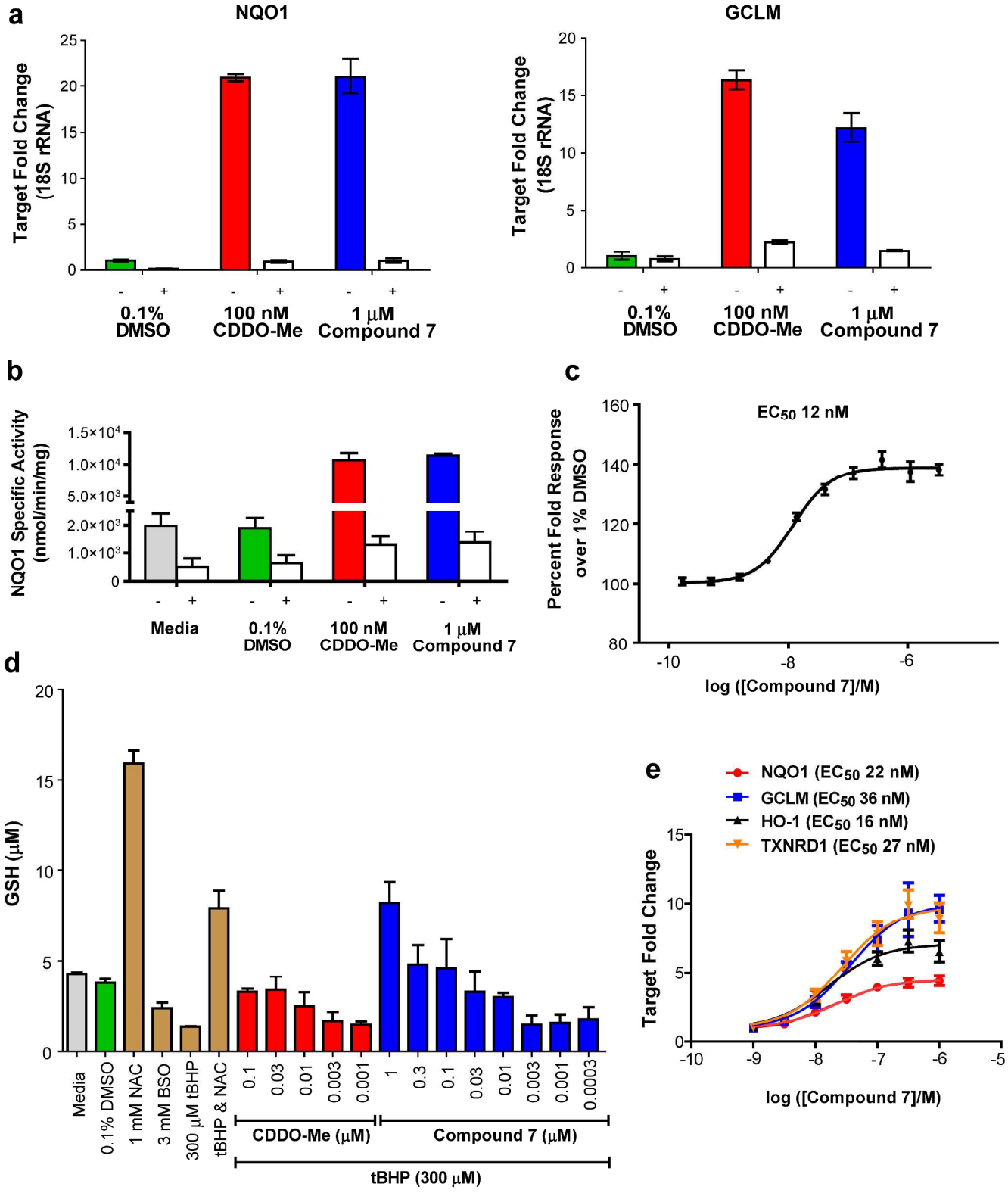
a
NQO1
Target Fold Change (18S rRNA)
0.1% DMSO
100 nM CDDO-Me
1 μM Compound 7
GCLM
b
NQO1 Specific Activity (nmol/min/mg)
Media
c
EC50 12 nM
Percent Fold Response over 1% DMSO
log ([Compound 7]/M)
d
GSH (μM)
Media
0.1% DMSO
1 mM NAC
3 mM BSO
300 μM tBHP
tBHP & NAC
CDDO-Me (μM)
Compound 7 (μM)
tBHP (300 μM)
e
NQO1 (EC50 22 nM)
GCLM (EC50 36 nM)
HO-1 (EC50 16 nM)
TXNRD1 (EC50 27 nM)
Target Fold Change
log ([Compound 7]/M)

Figure 5

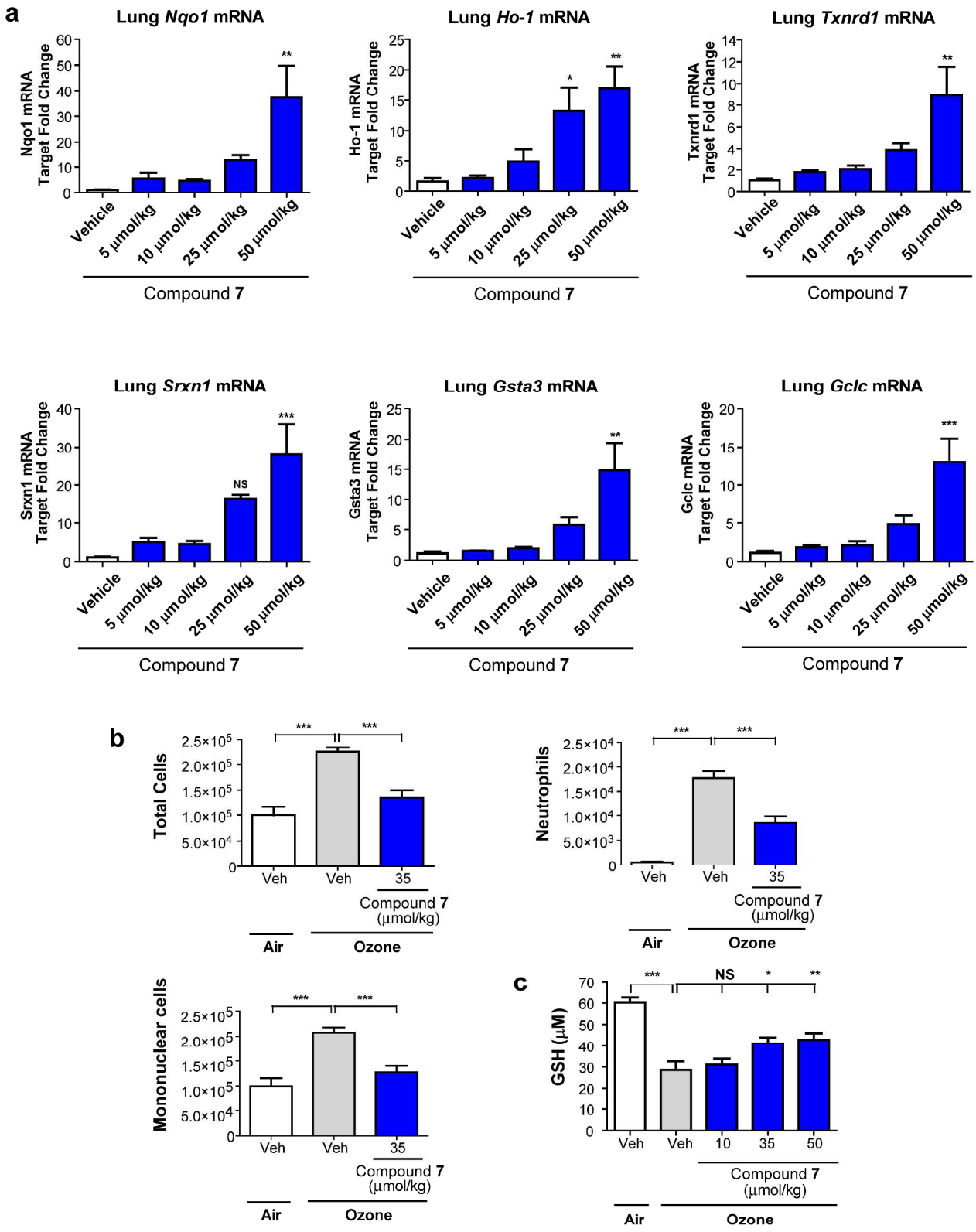
a
Lung Nqo1 mRNA
Nqo1 mRNA Target Fold Change
Lung Ho-1 mRNA
Ho-1 mRNA Target Fold Change
Lung Txnrd1 mRNA
Txnrd1 mRNA Target Fold Change
Lung Srxn1 mRNA
Srxn1 mRNA Target Fold Change
NS
Lung Gsta3 mRNA
Gsta3 mRNA Target Fold Change
Lung Gclc mRNA
Gclc mRNA Target Fold Change
Vehicle
5 μmol/kg
10 μmol/kg
25 μmol/kg
50 μmol/kg
Compound 7
b
Total Cells
Neutrophils
Mononuclear cells
Veh
35
Compound 7 (μmol/kg)
Air
Ozone
c
GSH (μM)
NS
10
50

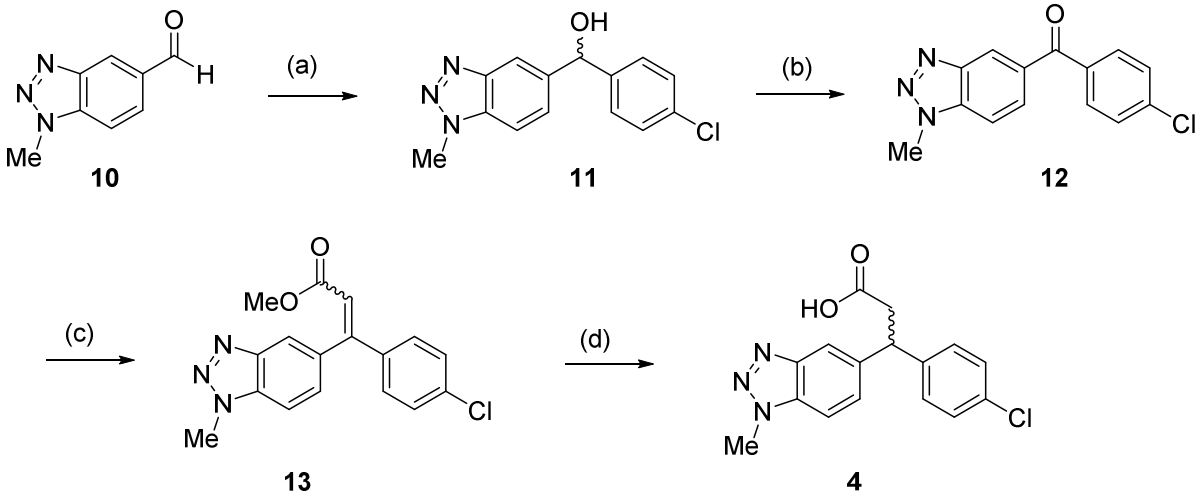

Scheme 1 (a) 4-Cl-PhMgBr, THF, 0°C, 94%; (b) Dess-Martin periodinane, DCM, 0°C, 76%; (c) $(MeO)_2P(O)CH_2CO_2Me$, tBuOK, THF, 0°C to RT; (d) $NiCl_2.6H_2O$, $NaBH_4$, MeOH, 0°C to RT, then aq. NaOH, RT, 50% over 3 steps.

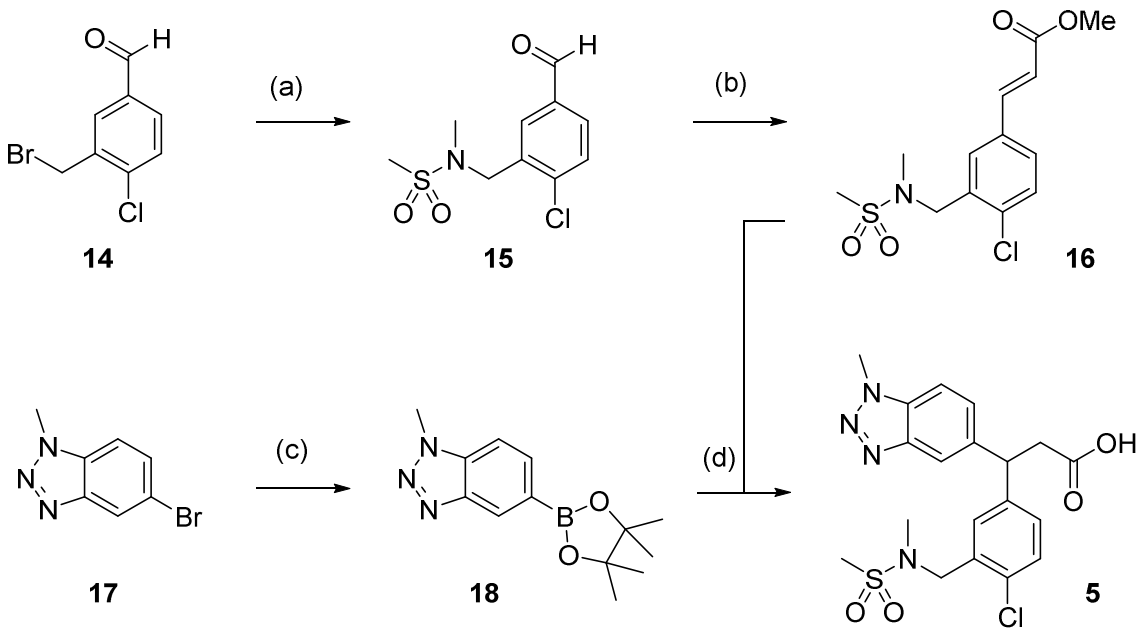

Scheme 2 (a) $MeSO_2NHMe$, K_2CO_3, MeCN; (b) $(MeO)_2P(O)CH_2CO_2Me$, tBuOK, THF, 0°C to RT, 92% over 2 steps; (c) bis(pinacolato)diboron, $PdCl_2$dppf, KOAc, dioxan, 90°C, 72%; (d) $[RhCl(cod)]_2$, Et_3N, dioxan, H_2O, 95°C, then LiOH, H_2O, RT; 17%.

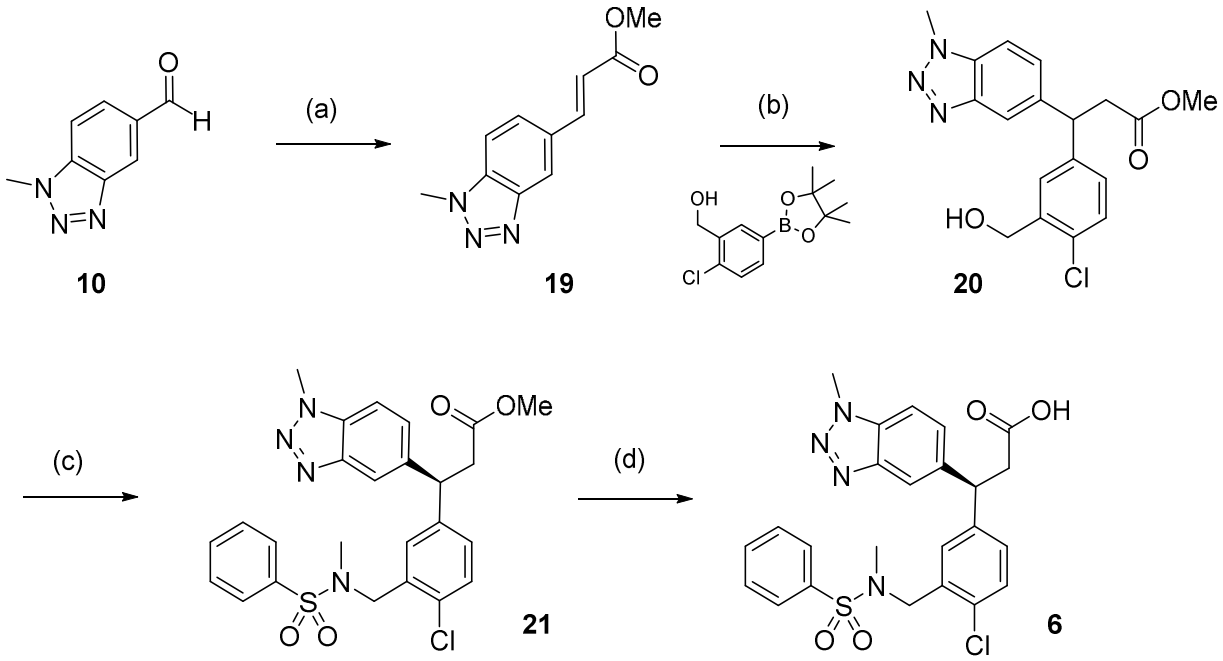

Scheme 3 (a) $(MeO)_2P(O)CH_2CO_2Me$, tBuOK, THF, 0°C, 78%; (b) $[RhCl(cod)]_2$, Et_3N, dioxan, H_2O, 95°C, 15%; (c) $PhSO_2NHMe$, $^nBu_3P$, ADD, THF, 0°C; then chiral HPLC; 15%; (d) LiOH, MeOH, H_2O, 80%.

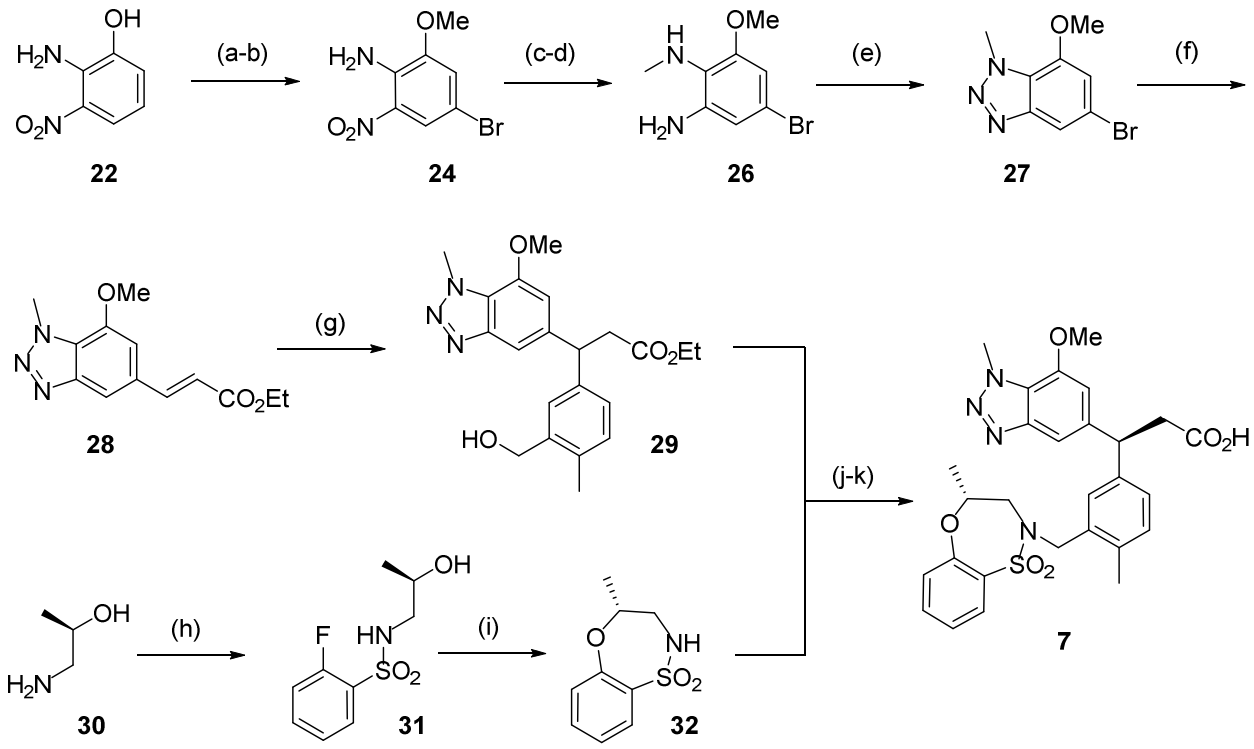

Scheme 4 (a) MeI, K_2CO_3, DMF, 89%; (b) Br_2, AcOH, NaAc, 95%; (c) MeI, NaH, DMF, 0°C, 72%; (d) Zn, AcOH, 28%; (e) $NaNO_2$, 10% aq. H_2SO_4, 36%; (f) Ethyl acrylate, $Pd(OAc)_2$, (o-Tol)$_3$P, DIPEA, DMF, 95°C, 83%; (g) $[RhCl(cod)]_2$, Et_3N, dioxan, H_2O, 95°C, 62%; (h) 2-F-$PhSO_2Cl$, K_2CO_3, THF, H_2O, quant.; (i) K^tOBu, DMSO, 100°C, 79%; (j) PS-PPh_3, DIAD, THF, 88%; (k) aq. NaOH, MeOH, then chiral HPLC; 26%.

FIGURE LEGENDS

Figure 1 The KEAP1 Kelch domain and NRF2-binding site. (a) Schematic of KEAP1 showing BTB, Intervening Region (IVR) and Kelch repeat (KR) domains. (b) Cartoon representation of the Kelch domain with a 9-mer NRF2-derived peptide bound. All figures in this paper depicting NRF2-bound KEAP1 were generated from the structure by Padmanabhan *et al* [24] (PDB code 1x2r). (c) Detail of the NRF2 ETGE motif, and its binding site on KEAP1. The Kelch surface is coloured by electrostatic potential as calculated by AstexViewer,[48] with regions of positive potential in blue and negative potential in red. (d) NRF2-site "hot-spots" identified from the fragment screen. Fragments for each hot-spot are shown in the context of the surface for the KEAP1-**1** structure, which is coloured according to binding footprint. The side-chain of Arg 415 was excluded for clarity. (e) Chemical structures for the three fragment hits discussed in the text. (f) Interactions between fragment **1** (green bonds) and the Kelch domain. The final $2mF_o$-DF_c electron density (contoured at 1σ) is shown as a blue mesh. The bound structure of the 9-mer NRF2 peptide (orange bonds) is overlaid for comparison. (g) Overlay of binding site surfaces for NRF2-bound Kelch domain (orange) and for the Kelch domain bound to fragment **1** (white) showing remodelling of the site upon ligand binding. Fragment **1** is shown as a green surface.

Figure 2 Structure-driven elaboration of fragment **1**. (a) Overlay of fragments **1** and **2** bound to the Kelch domain in the context of the elaborated compound **4**. The benzotriazole superposes well with the heterocyclic system of fragment **2**. Protein-ligand hydrogen bonds are depicted by dashed lines. (b) Overlay of fragment **3** bound to Kelch with compound **5** showing superposition of their sulfonamide moieties. (c) Overlay of fragment **1**, and compounds **4** - **6** bound to the Kelch domain illustrating step-wise growth of the anchor fragment. Protein is shown for the KEAP1-**6** structure. (b) Surface representation of the NRF2-binding site of KEAP1 with

compound **7** bound. The final $2mF_o$-DF_c electron density (contoured at 1σ) is shown as a blue mesh. (c) Schematic representation of interactions formed between compound **7** and the NRF2-binding site of Kelch. The three-point pharmacophore (acid, aromatic-acceptor and sulfonamide) identified during the fragment screen is highlighted and coloured as in Figure 1d. (d) Isothermal Titration Calorimetry (ITC) data for compound **7** and its interaction with the Kelch domain (K_d reported in Table 1).

Figure 3 Comparison of NRF2 and compound **7** interactions with KEAP1. (a) Overlay of the KEAP1-bound pose of the 9-mer NRF2 peptide (orange carbon atoms) and compound **7** (green carbon atoms). Peptide residues are labelled with their single amino acid code, and hydrogen bonds are depicted by dashed lines. (b) Compound **7** mimics the electrostatic interaction between Glu 79 of NRF2 and Arg 483 and (c) between the NRF2 peptide backbone and Tyr 525/Gln 530/Ser 555. The protein structure is that for the KEAP1–**7** complex. (d) Surface representation of compound **7** bound to the KEAP1 Kelch domain. Compound **7** exhibits high shape complementarity with the NRF2-binding pocket and completely fills the site. The bound pose of the NRF2-derived peptide is overlaid for comparison.

Figure 4 *In vitro* activation of the NRF2 pathway by compound **7**. "-" signifies non-targeting control siRNA, "+" signifies *NRF2* siRNA treatment. (a) Treatment with compound **7** for 24 h leads to an increase in *NQO1* (left panel) and *GCLM* (right panel) mRNA expression in an NRF2–dependent manner in NHBE cells. The graphs illustrate the mean target fold change of three samples (n=1 experiment, mean ± 95% CI). The data are representative of 2 studies. (b) compound **7**-induced NQO1 enzyme activity is NRF2-dependent. Data are representative of two studies using two different NHBE cell donors (mean ± SD). (c) Compound **7** increases NQO1 activity in a concentration-dependent manner in BEAS-2B cells (n=3 experiments, mean ±

SEM). (d) Compound **7** pre-treatment prevents tBHP-induced depletion of GSH in a concentration-dependent manner in NHBE cells (mean ± SD). Data are representative of 3 experiments. (e) Compound **7** increases the expression of NRF2-regulated genes in a concentration-dependent manner in COPD patient-derived epithelial cells (mean ± 95% CI). Data are representative of 2 donors.

Figure 5 *In vivo* activation of the NRF2 pathway by compound **7** (IV infusion). (a) Compound **7** induces dose-dependent increases in the expression of NRF2-regulated genes in rat lung tissue *in vivo* (mean ± SEM). One-way ANOVA with Dunnetts correction; **P*<0.05; ***P*<0.01; ****P*<0.001 versus Vehicle. (b) Compound **7** attenuates ozone-induced increases in rat BAL fluid leukocyte numbers *in vivo* (mean ± SEM). One-way ANOVA with Dunnetts correction; **P*<0.05; ***P*<0.01; ****P*<0.001. (c) Compound **7** restores the ozone-induced depletion in pulmonary GSH levels in the rat *in vivo* (mean ± SEM). One-way ANOVA with Dunnetts correction; NS = not significant; **P*<0.05; ***P*<0.01; ****P*<0.001 versus Ozone + Vehicle.

Table of Contents graphic